Università degli Studi di Ferrara
Facoltà di Scienze Matematiche, Fisiche e Naturali

Dottorato di Ricerca in Fisica

Ciclo XXV

Image spectroscopy for diagnostic and conservation of contemporary art materials

Dr. Virginia Pellicori

Settore Scientifico Disciplinare FIS/07

Tutor
Prof. Mauro Gambaccini

Advisor
Prof. Ferruccio Petrucci

Coordinator
Prof. Vincenzo Guidi

Referees
Prof. John Delaney
Prof. Daniela Comelli

Anni 2010/2012

Contents

Introduction

To works of art is often assigned a specific value of cultural and expressive testimony of an artist or, more generally, of a culture.

Preserve this value means keeping intact the appearance of the work, its component material in order for the message to reach the public, without alteration.

A good knowledge of the materials constituting the work is needed to preserve them appropriately.

This work is focused on the study of modern and contemporary paintings and of materials used, which can be distinguished in supports, pigments, binders, varnishes, each one with a peculiar behavior and a specific way of interacting with other materials and with external agents.

While much is known about traditional materials and the way they are aging, modern and contemporary materials are not well known. They are mainly synthesis materials and is often difficult to obtain their exact composition by the manufacturers. Sometimes the name remains the same while the product is modified.

The main goal of this work is to investigate some of the most popular art materials to track even the weakest changes, which are index of degradation and occur in the form of chromatic alterations.

Image spectroscopy is the scientific technique on which we focus our attention, since it helps to reveal early alterations using reflectance imaging, in a complete non-invasive way. Spectral data are processed by multivariate analysis, in a very efficient way.

Other scientific methodologies have been used to the same purpose. X-ray fluorescence is used to collect more detailed information about the materials. Colorimetric analysis has been performed to study alteration trends. Image diagnostics, as Ultraviolet fluorescence, Wide band infrared reflectography, have proved useful to collect information on the state of conservation of works in non-quantitative way.

The common features of such techniques are to be non-invasive, non-destructive, to be used *in situ*. These are common requirements for monitoring periodically works of art.

Chapter 1

Multispectral reflectance imaging

To preserve adequately the work of arts effective scientific methodologies have been developed in order to investigate the polimateric and complex structure of painting. An effort has been made for non-destructive and non-invasive diagnostics, as well as for instruments performing *in situ* analysis.

Techniques available in Archaeometry Lab at Department of Physics and Earth Sciences of Ferrara University, will be taken into consideration in the following.

The protocol of examination foresees the analysis of a painting by image diagnostics, followed by spectroscopic techniques. Attention is focused on Image Spectroscopy (IS), discussed in depth in the next chapters.

1.1 Structure of the paintings

The propagation of the electromagnetic radiation in a painting depends on the physical features of the pictorial layers. In Western art, the painting structure has changed over time. In Middle Age a painting was executed according to the *regola d'arte*, following specific rules and recipes, ensuring a correct preservation of the work, according to previous experience. Art, since 19^{th} century moved against this tradition, and the twentieth century is characterized by a lot of artistic experimentations and new ways of representing the reality. The general rule became the free expression of the individual artist.

The structure of a painting (Fig. 1.1) is usually composed by:

- *Support*: Until the XV century it was constituted by a wood panel [14]. Often, it was covered by a canvas to limit the wood movements due to humidity variations. Then it was replaced by a canvas support, since it was of lightweight, easily transportable, suited to host the paint film. Other widely diffused typologies of support are the paper and wall. The old paper differs greatly from the modern, because production techniques changed. Originally

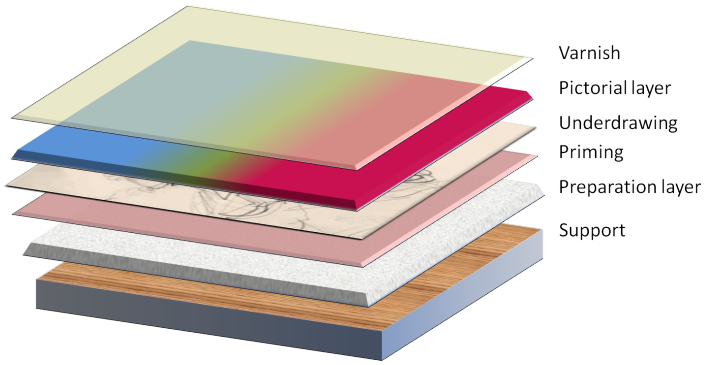

Fig. 1.1: Structure of a painting.

the paper was produced from rags, from which the cellulose was obtained. The modern paper is produced from the wood, making it much acid for the high percentage of lignin and more susceptible to degradation for the shorter cellulose chains. This involves that the modern and contemporary works on paper are more fragile.
The most common technique on the wall is the fresco; the others are mural, graffiti, encaustic. The fresco is one of the painting techniques more resistant to degradation. Greek, Etruscan and Roman frescoes have come down to us.

- *Preparation layers*: In the Middle Age, it was constituted by chalk and animal glue. Sometimes, a last layer of *priming* was applied as a base. The priming became a colored preparation used to emphasize the pictorial film overlying, during 16^{th} century [22].
  Concerning the frescoes, the wall needed to be adequately prepared to host the painting. The first preparation layer, called *arriccio*, consisted of fat lime and coarse sand. On the *arriccio* was spread a thin layer of plaster, called *intonachino*, composed of lime and fine sand, intended to receive the color.

- *Preparatory drawing*: In paintings on wood or canvas, the preparatory drawing was executed with black pigment applied by brush or stick.
  In the fresco, the drawing was spread on the *arriccio* by red ocher, called *sinopia*, then covered by *intonachino* layer. From the end of XV century and early XVI century the use of cardboard became widespread to reproduce the drawing directly over the *intonachino* layer [21].

- *Pictorial layers*: mixture of pigments and binder. Originally, the pigments were earths and minerals finely pulverized or organic dyes. Nowadays and since, they are principally synthetic pigments. Their particle sizes affect the propagation of the radiation in the pictorial layer and so the final features of the layer. Concerning the binders, the most used were the drying oils (oil painting), as the linseed oil, poppy seed oil and walnut oil, that replaced the egg yolk (egg tempera painting) almost at the same period of the spread of

canvas. For the tempera painting other used binders were glue, honey, wax, water, milk (in the form of casein) and a variety of plant gums. In recent times, synthetic binders as acrylic, alkyd, vinyl resins, are usually used.
For painting on paper, the main techniques that use paper as support are the watercolors and the pastels, but also tempera or mixed techniques. In the watercolors, the finely ground pigments are mixed with the binder, the Arabic gum, and diluted in water. Pastels, used since the end of XV century, consist of pure powdered pigment and Arabic gum as traditional binder. Methyl cellulose was introduced as a binder in the twentieth century [21].
In fresco, not every pigments were used, due to the action of caustic lime. Pigment of mineral origin, as calcium carbonate, ochers, earths, were preferred. They were applied when the plaster is still wet, hence the name "fresco" (fresh). Thereby the pigment particles, exploiting the chemical reaction of plaster with the air, were completely incorporated in the layer of plaster. Compared to "secco" mural painting techniques, in which the pigments were applied on dry plaster, it was much more resistant to degradation. Frequently the finishing retouches were applied by *a secco painting*, through the use of tempera [36].

- *Varnish*: It is the final layer of a painting, colorless, applied to protect the pictorial layer.

1.2 Studying paintings by image diagnostics

The structure of paintings, previously described, determines a complex variety of interactions between electromagnetic radiation and painting layers. As a result of such interactions, some information on the chemical nature of the compounds as well as on the physical features of the painting can be achieved by means of scientific techniques.

The image diagnostics in the visible range are useful to provide the photographic documentation in diffuse light and an overview of the state of conservation.

The *macro-photography* is useful to observe and document, at high magnification, relevant dimensional details of painting.

The survey in *raking light* highlights the three-dimensionality of pictorial surface (Fig. 1.2(a), 1.2(b)). It can reveal the warp of support, the tension state of the canvas, the brushstroke trend, the *craquelure* features, and other significant aspects of the condition of the painting.

The *trans-illumination*, based on image acquisition of light transmitted through the painting, is used to investigate the transparency of layers and the presence of rips or tears on the support (Fig. 1.2(c)).

The radiations at non-visible wavelengths can reveal other aspects of the paint-

(a)

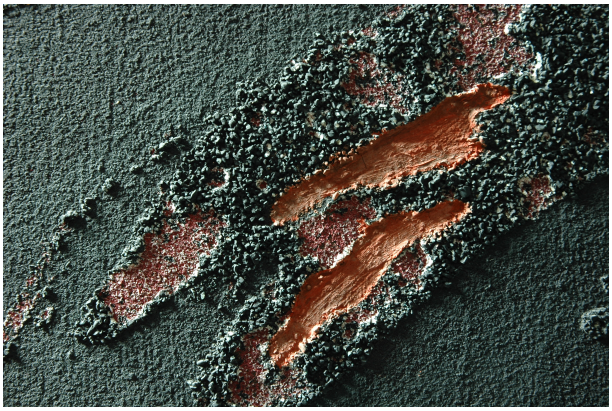

(b)

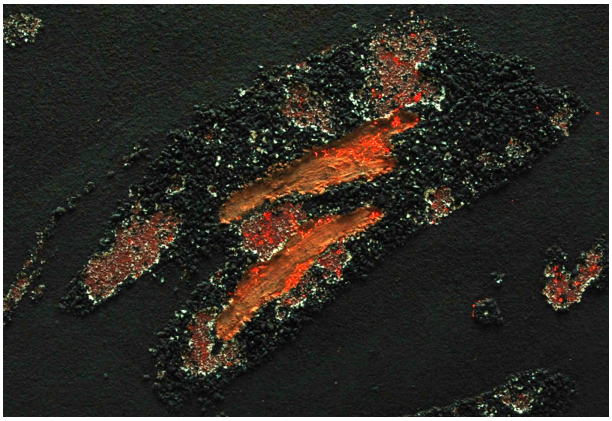

(c)

Fig. 1.2: Giulio Turcato, *Untitled*, 20^{th} cent. Mixed technique on canvas, 50x70 cm, Remo Brindisi Casa Museo, Comacchio (FE). (a) Diffuse light photography (b) Detail in raking light (c) The same detail in trans-illumination.

ing.

The *ultraviolet fluorescence* is widely used as an investigation method of painting surfaces. It allows to capture the fluorescence emissions of the materials due to radiative de-excitation, through the illumination of the work with ultraviolet radiation. The ultraviolet source generally employed is a Wood lamp. The UV light is used to exicite both pigments and media (such as paint binders and varnish layers). The emitted light is at a lower energy than the incident light thus it is red shifted in color. Phosphorescence phenomena can be also occur by UV absorption, giving rise to luminescence from the painting. The interpretation of an image in fluorescence generally concerns the identification of diversified situations characterizing the work surface, as the presence of different type of varnish, distinguishable for their aging, or retouches, which usually appear as darker areas. In some cases, pigments are differentiated, although appearing similar under visible light [1]. In the painting shown in Fig. 1.3(a), the yellow pigments become distinguishable under UV irradiation, by manifesting two distinct fluorescence emissions (Fig. 1.3) [4]. More recently new perspectives on the application of ultraviolet fluorescence have been opened [37].

Many studies are devoted to the luminescence in the near-infrared spectral region, as in the case of cadmium pigments [34] or of the Blue Egyptian in ancient artifacts [38].

Increasing the wavelength, the scattering phenomena show a sharp decrease, so that the covering power is reduced and the pictorial layers become transparent to the radiation. This means that the investigation in the near infrared range makes visible layers beneath the paint film [22].

Thus, the *infrared reflectography* is a well-known tool to study the pictorial technique used by the artist, the possible presence of underdrawing, the use of brush or charcoal, *pentimenta* (Fig. 1.4) and retouches, the presence of the artist signature [6]. It can be performed by a camera based on Silicon CCD detector to gather information in the 800-1100 nm spectral range. By using devices, like InGaAs detectors, sensitive to longer wavelengths up to 2,5 μm, additional information can be obtained [12].

X-ray digital radiography takes advantage of the high penetrating power of x-rays to investigate the materials crossed by the radiation. The X-ray radiography is thus the most suitable technique to analyze works at high thickness, like the wooden panels. The X-ray can provide information on the state of conservation of both support and pictorial layers. This technique may be reasonably considered complementary to IR reflectography, revealing paintings hidden by a thick paint film (Fig. 1.5) [5].

The radiographic contrast is due to different *radiopacity* (that expresses their ability to attenuate radiation) of materials interacting with X-rays. It depends on the atomic number of the elements constituting the compounds, their density and thickness [6].

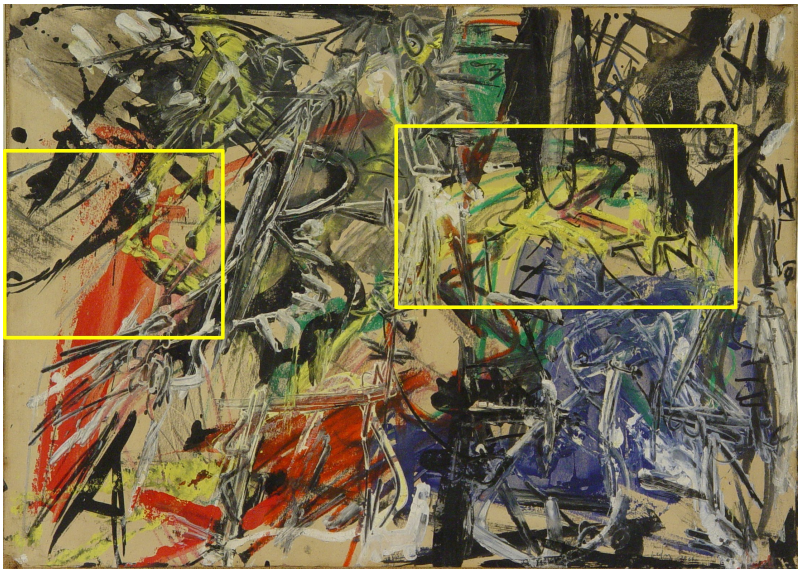

(a)

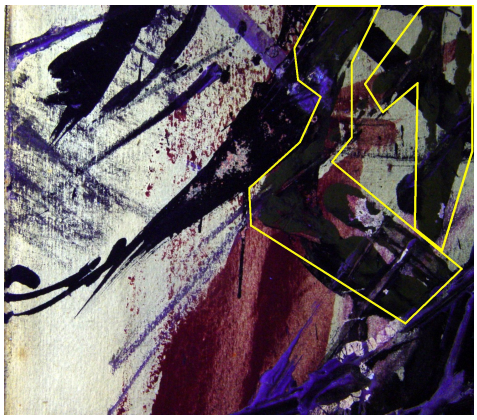

(b)

(c)

Fig. 1.3: Emilio Vedova, *Untitled*, 1961, painting on paper on canvas, 35x49 cm, Remo Brindisi Casa Museo, Comacchio (FE). (a) Diffuse light photography; (b) (c) UV induced fluorescence details of the two yellow pigments.

(a)

(b)

Fig. 1.4: Giorgio De Chirico, *Ettore e Andromaca*, 1958, painting on canvas, 70x60 cm, Remo Brindisi Casa Museo, Comacchio (FE). (a) Image in diffuse light (b) Detail in Infrared reflectography.

(a)

(b)

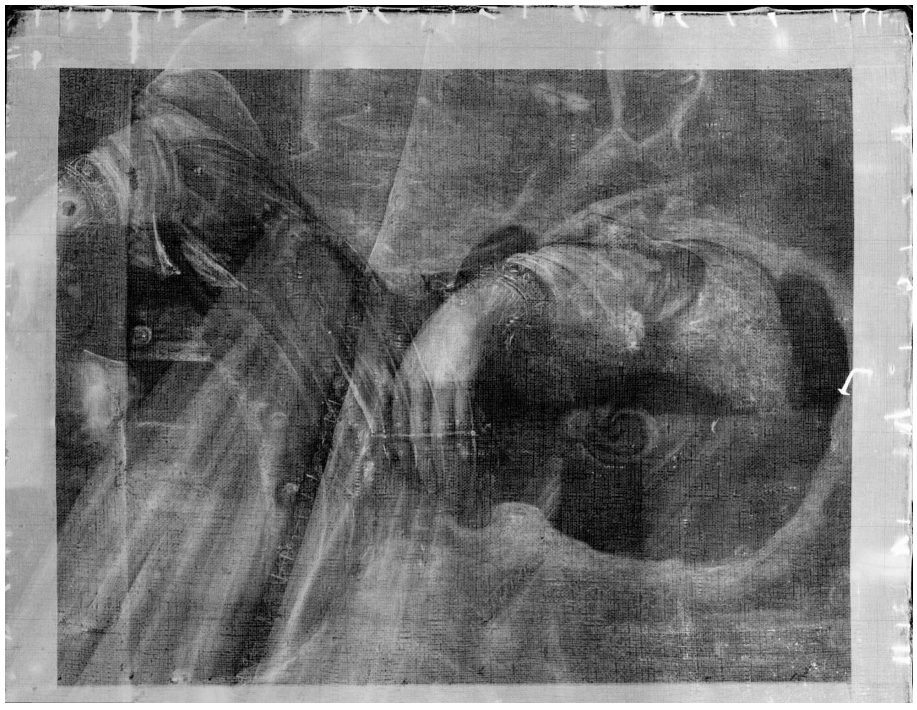

Fig. 1.5: Portrait of Giacomo Masino, second half of XVI cent., painting on canvas, private collection. (a) Image in diffuse light (b) X-ray radiography - image rotated by 90 °.

1.3 Studying painting materials by spectroscopic methods

Spectroscopic method are more and more employed to the aim of identifying pictorial materials or their degradation, in a non-invasive fashion.

The most widely used in cultural heritage field is the *X-ray fluorescence*. The registered spectrum consists of the emission lines of characteristic X-ray fluorescence of the atoms, induced by irradiation with X radiation [39]. It makes possible to recognize the presence of element with atomic number greater then 13 of the investigated work [32]. XRF analysis is more effective when its results are compared with those from the optical methods, by making it possible to discriminate among pigments of similar.

The *VIS spectrophotometry* can be used for accurate and precise result in the visible range, returned as reflectance spectrum, in which the tens of points recorded provide the reflectance per unit wavelength. The measurement of color can be done also by *colorimetry*, which specifies the color in numeric terms by means of three colorimetric parameters. Both methods are effective to monitor color changes and the deterioration occurring on paintings. The disadvantages attributable to such analysis are the need of contact with the sample surface and the analysis of small area. Since the works of modern and contemporary art are often highly textured, they can be difficult to analyze with contact.

The *Image Spectroscopy (IS)*, allows to collect simultaneously spatial and spectral information, expanding the effectiveness of both image diagnostics and spectroscopic techniques. By collecting images at different wavelengths, the reflectance spectrum is subsequently obtained. IS can help in the choice of points to be analyzed by contact spectrophotometry and XRF for colorimetric and elemental analysis, respectively. A comparison between the spectrophotometry and the image spectrophotometry was made by Berns [11], by evaluating the performances of various approach to spectral imaging. The advantages provide by the spectral imaging were highlighted, demonstrating a reasonable correlation between the two methods, with opportunities to further improve the system.

The spectral imaging is of recent application on cultural heritage field. It was initially developed in astrophysics and geophysics for Earth remote sensing [19] and then extended to military purposes. Afterward, thanks to the advancement of research and technology, also the other sciences are involved in the use of spectral imaging [17]. Since the 1930s and more considerably in recent years, the spectral imaging technology has been extended in the field of conservation of artworks [9].

The first spectral imaging system used at Physics Department in Ferrara University was *NIR1000*[1], characterized by sixteen interferential filters and a analog Silicon CCD camera [28]. Several improvements have been made in the following

[1] *NIR1000* by Spectra Elettronica, Milan, Italy.

years (Fig. 1.6), making it possible the development of the actual system, used in this work to perform reflectance measurements without contact on paintings.

Fig. 1.6: Image spectroscopy apparatus, developed in the first years of 2000.

Chapter 2

Instruments and analytical tools

The scientific instruments presented here are used with the purpose to investigate works of art in noninvasive way to obtain information on their state of conservation and on constitutive materials.

VIS-NIR reflectance spectra are achieved by Image Spectroscopy (IS) and by Spectrophotometry with integrating sphere.

Sequences of images acquired by IS highlight possible reflectance changes at different wavelengths.

IS spectral data are examined through the Principal Component Analysis (PCA) to detect weak color changes, performing an effective monitoring. Finally, colorimetric analysis can help in the identification of the alterations trend.

2.1 Measurements of diffuse reflectance

The reflection of light by a painting layer can contain the *specular* and / or *diffuse components*.

The *specular reflection* occurs when part of the radiation is reflected from a flat surface only in the direction which forms an angle equal to that of incidence with respect to the normal to the surface, and the incident and reflected beams lie on the same plane (Snell's laws).

The *diffuse reflection* represents the radiation reflected by the sample in all directions, without a favorite direction. It is due to the surface roughness and to the penetration of radiation in the layer itself (Fig. 2.1)[33].

This is also called *volume reflection* because it consists in the radiation which comes out in random directions as a result of multiple reflections, refractions, transmissions and scattering inside the sample (Fig. 2.2). The radiation is diffusely reflected according to the shape, the size, the orientation and the concentration of the particles inside the sample as well as to the thickness of layers. Such reflections

and *selective absorptions* occur at wavelengths bands correlated to the pigment nature.

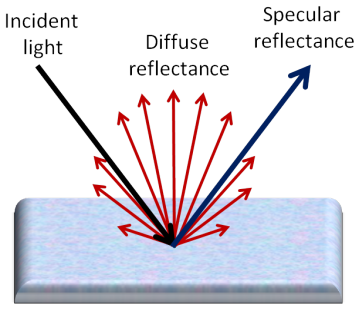

Fig. 2.1: Representation of surface reflectance with specular and diffuse components.

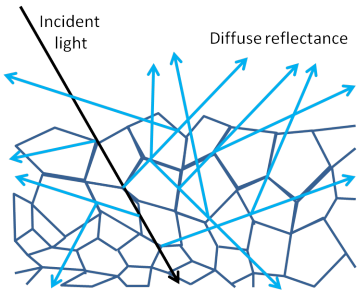

Fig. 2.2: Representation of volume reflectance with specular and diffuse components.

The diffuse reflectance is defined as

$$\rho_\lambda = \frac{I_{RD}}{I_0}$$

where:
I_{RD} is the diffusely reflected radiation and I_0 is the intensity of the incident radiation. The diffuse reflectance depends on the geometry of illumination and collection of light, which will be exposed with more detail below. It is a dimensionless quantity. In the VIS-NIR range it allows to investigate the pictorial layers, without perform sampling.

The diffuse reflectance measurements can be carried out through an integrating sphere or a remote sensing system. The integrating sphere is coated with a highly reflective and diffusing material to the aim of diffusing uniformly and isotropically the incident light on the inside as well as gather all the light reflected by the sample placed on one sphere aperture. The use of integrating sphere for spectral measurements gives high accuracy and repeatability to the results. However, the accuracy is affected by the geometric conditions of incident and absorbed radiation.

Generally, the measurement geometry is specified by means of polar coordinates system, centered at the point O on the specimen surface and with azimuthal angles referred to an appropriate direction on the specimen (Fig. 2.3):

- ε_1 is the angle between the perpendicular to the specimen (axis z) and the direction of incidence;
- ε_2 is the angle between the perpendicular to the specimen (axis z) and the direction of observation;
- φ_1 is the angle between a reference axis (axis x) and the plane of incidence;
- φ_2 is the angle between a reference axis (axis z) and the plane of observation [31].

The angles of aperture of incident beam ($2\sigma_1$) and of the observed beam ($2\sigma_2$) are also considered (see Appendix). In the case of hemispherical illumination and observation, obtained with integrating sphere, the respective solid angles correspond to 2π. The light is, thus, diffused and the angle is indicated with "d".

In the case of directional illumination and observation, the respective solid angles correspond approximately to 0.

In the real situation, the illumination and observation beams show a solid angle more or less large.

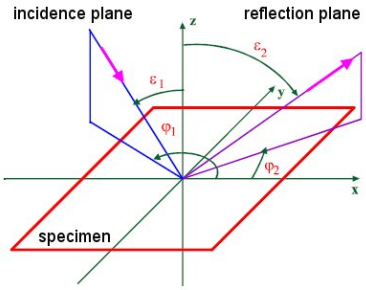

Fig. 2.3: Polar coordinate system for the spectrophotometric measurements.

The measurement geometries are distinct in relation to the applications. Those most widely used for reflectance measurements are shown in Table 2.1 [24]. The integrating sphere fitted on the spectrophotometer used in this work, has d/8° configuration. Therefore, the incident light is diffused by the integrating sphere and subsequently collected by detector, with an angle of about 8 degrees. The reflectance measurements performed by IS, which will explained with more detail hereafter, use a 2x45°/0° geometrical configuration, ensuring the exclusion of specular component of the reflected radiation.

Such measurements needs a calibration with reference standards, used as ideal reflecting diffusers. Their reflectance values were certified by using 0°/d SPINC

Geometry	Irradiation		Observation		Specular reflection	CIE quantity	Quantity symbol
	ε_1	σ_1	ε_2	σ_2			
0/d SPINC	± 10°	± 5°	diffuse	diffuse	included	reflectance	$\rho_{0/d}$
0/d SPEX	± 10°	± 5°	diffuse	diffuse	excluded	diffuse reflectance	$\rho_{0/ds}$
d/0 SPINC	diffuse	diffuse	± 10°	± 5°	included	reflectance factor, d/0	$R_{d/0}$
d/0 SPEX	diffuse	diffuse	± 10°	± 5°	excluded	reflectance factor, d_s/0	$R_{ds/0}$
45/0	45°± 2°	± 8°	± 10°	± 8°	excluded	reflectance factor, 45/0	$R_{45/0}$
0/45	± 10°	± 8°	45°± 2°	± 8°	excluded	reflectance factor, 0/45	$R_{0/45}$

Table 2.1: CIE geometry of irradiation and observation for reflection measurements and relative quantities. SPINC indicates the included specular component, while SPEX the excluded specular component.

geometry (including specular component), established by *Commission International de l'Eclairage* (CIE) [24].

Therefore, the result of IS measurements represents a relative quantity, called *spectral reflectance factor* R_λ, which is expressed by the ratio between the detected radiation diffused from the sample I_{RD} and the intensity of the radiation reflected by reflectance standard I_{ref}[15]:

$$R_\lambda = \rho_{ref} \frac{I_{RD}}{I_{ref}}$$

where
ρ_{ref} is the certified value for the reflectance standard.

This equation, generally valid for the visible range, can be extended up to NIR range, since until 2.5 μm thermal emission is negligible.

2.2 Image Spectroscopy

IS is based on the digital acquisition of images at different wavelengths in the visible and near infrared spectral range (410-970 nm) to obtain spectral reflectance factor with no contact with surfaces.

A Pulnix TM-1325 $CL^{©}$ monochrome digital camera with a 2/3" interline transfer CCD of 1392 x 1040 pixel is employed. An optomechanical device has been designed and built by the collaboration between INFN – Section of Ferrara and Ferrara University[1]. A narrow band optical filter is placed in front of camera

[1]S. Chiozzi, F. Evangelisti, S. Squerzanti, of INFN – Section of Ferrara, and L. Landi of Ferrara University

for spectral selection of light (Fig. 2.4). Fifteen interferential filters 1" in diameter, 10 nm FWHM bandwidth (discussed in more detail in Section 3.1.3) are used for multispectral imaging (Fig. 2.5). Spectral data are thus collected with about 40 nm sampling pitch. This interval is reduced in the spectral region between 670 and 750 nm, since it is useful for a particular case of recognition of pigments in the visible range (see Sections 4.2, 4.3). Such system is fitted with a Nikon AF Nikkor 50 mm, f#1.8 lens.

(a) 

(b) 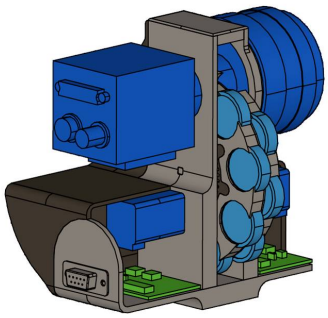

Fig. 2.4: Image spectroscopy device, equipped with Pulnix TM-1325 CL camera (a) and its internal structure (b)

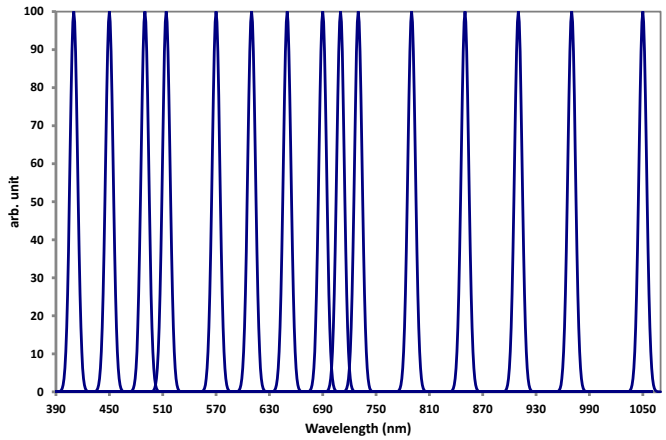

Fig. 2.5: Representation of 10 nm pass-band filter transmission, covering the VIS-NIR spectral range

To ensure a diffuse illumination, a pair of 650 W halogen lamps mounted in diffusing spotlights are used to light the subject symmetrically. Light is collected by IS device, in 2x45°/ 0° geometrical configuration (Fig. 2.6, Fig. 2.7). Seven Spectralon diffuse reflectance standards[2], 2%, 5%, 10%, 20%, 50%, 75%, 99%, are included in every captured scene as references for reflectance determination.

[2] *Spectralon*® diffuse reflectance standards by *Labsphere*©

Their reflectance values in the VIS-NIR range are measured by contact spectrophotometer CM2600-d and extrapolated in the 750 - 1050 nm band, according to the certified values supplied by the *Labsphere*© 50 nm with spectral pitch within a standard deviation of 0.5 (Fig. 2.8). The measured RMS noise calculated for the 2%, 50%, 99% diffuse reflectance standards in an acquired image at 650 nm is respectively of 0.90, 1.95 and 0.66 reflectance percentage points.

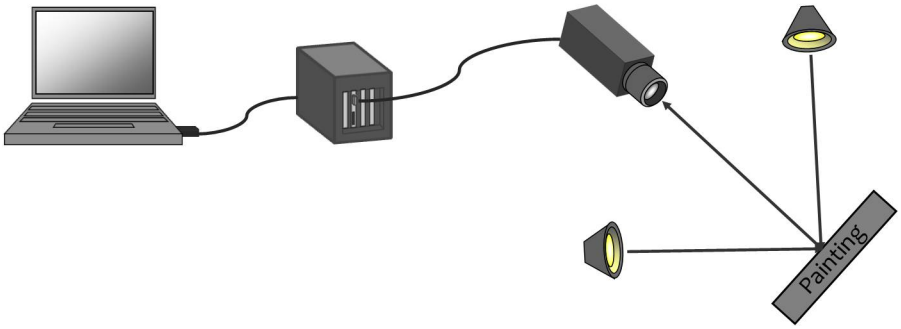

Fig. 2.6: Image Spectroscopy set up.

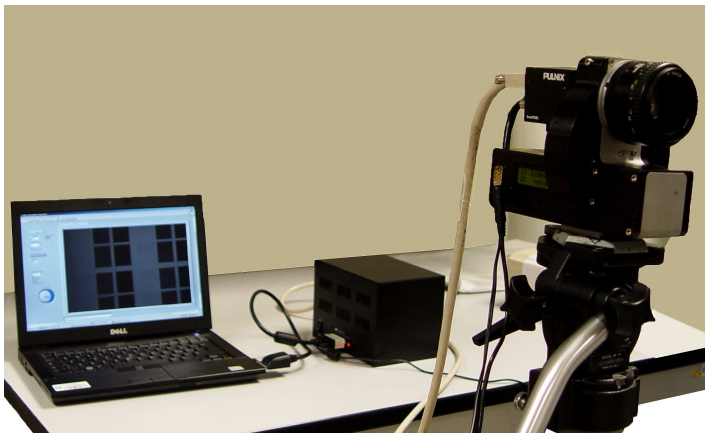

Fig. 2.7: Portable Image Spectroscopy apparatus.

Up to fifteen images may be acquired and stored as 8-bit TIFF files in a complete IS session. Each image is averaged over 20 frames to reduce random noise. Filter change is driven by RS232 serial line. The same set up is used for the acquisition of white field images of a smooth cardboard to correct non-uniformity. Images are captured and registered by a National Instrument NI PCI-1428 frame grabber, driven by dedicated software, developed in *Labview*© platform. The PCI card is hosted in a metal case and coupled by PCI-express card to a notebook[3] (Fig. 2.7). Processing of the image sequence to construct the data cube is made

[3]Express card for expansion box to notebook, by EXSYS Vertriebs GmbH

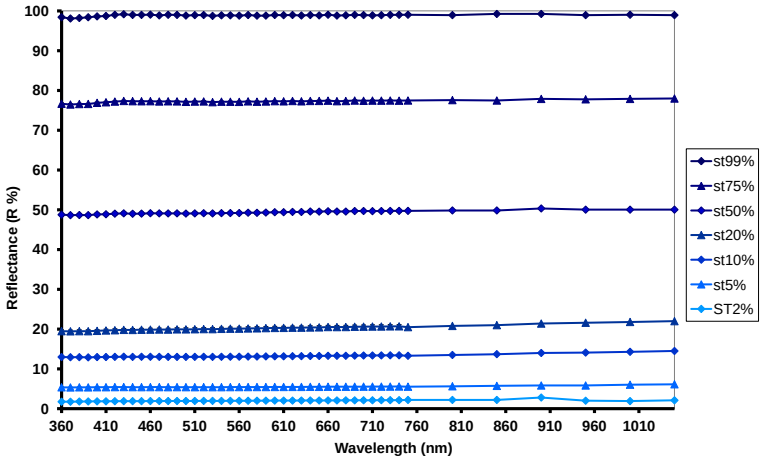

Fig. 2.8: Reflectance of S*pectralon*® standards in the VIS-NIR range.

by Tele32 software[4] (Fig. 2.9). Portability and flexibility are distinctive features of this device, designed to perform *in situ* Image Spectroscopy sessions. Some design choices, like the adoption of widely used standards for mechanical coupling with lens and camera and the easy replacement of optical filters, make this apparatus particularly efficient for conservation issues.

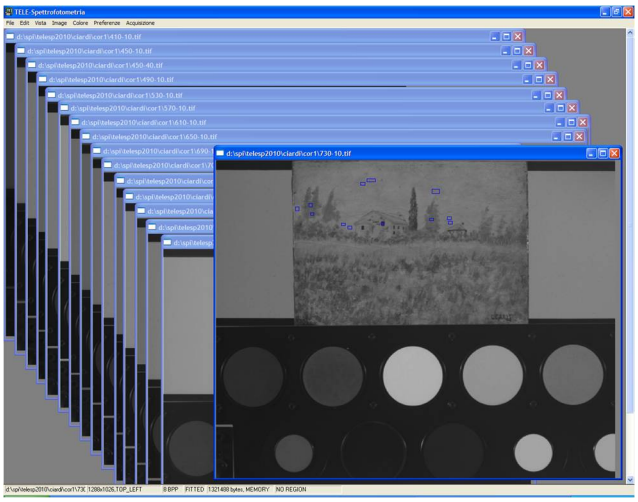

Fig. 2.9: Graphical user interface of Tele 32 software with the acquired images at different wavelengths

[4]Tele32, by I. Bortolotti

2.2.1 White-field

To correct for uneven illumination, optical defects and other non-uniformity of the images, white field images are acquired with the same acquisition conditions of the IS sequence, like distance from work, illumination, lens aperture and focus. The correction of each pixel (x, y) in an image is done by the following algorithm:

$$I_\lambda(x,y) = i_\lambda(x,y)\frac{< \overline{b_\lambda(x,y)} >}{b_\lambda(x,y)}$$

where:
$I_\lambda(x,y)$ is the corrected image;
$i_\lambda(x,y)$ is the image to correct;
$b_\lambda(x,y)$ is the white field image;
$< \overline{b_\lambda(x,y)} >$ is the mean value of white field gray levels.

Thereby, the ratio between gray level value for each pixel of $i_\lambda(x,y)$ image and the same pixel value of $b_\lambda(x,y)$ image is calculated.

2.2.2 Reflectance factor calculation

After image correction, interpolation is need to achieve a quantitative reflectance measurement. One reference region of interest (ROI) for each S*pectralon*® reflectance standard is selected (Fig. 2.10). The mean value of gray levels in the ROI is calculated.

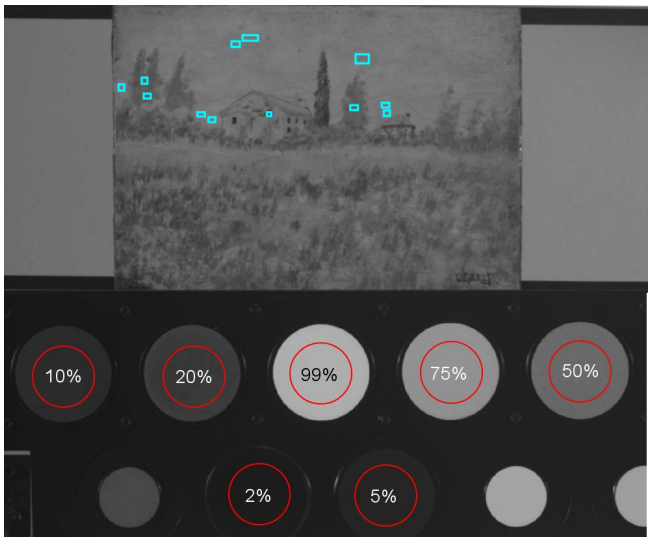

Fig. 2.10: Reference (red lines) and measurement region of interest (blue lines).

Interpolation between the gray level values and the reflectance values (Fig. 2.8) is performed by using a third-degree polynomial. This curve is used to interpolate

spectral reflectance factors on any ROI (Fig. 2.11). This procedure is repeating by software for all acquired images in the subject.

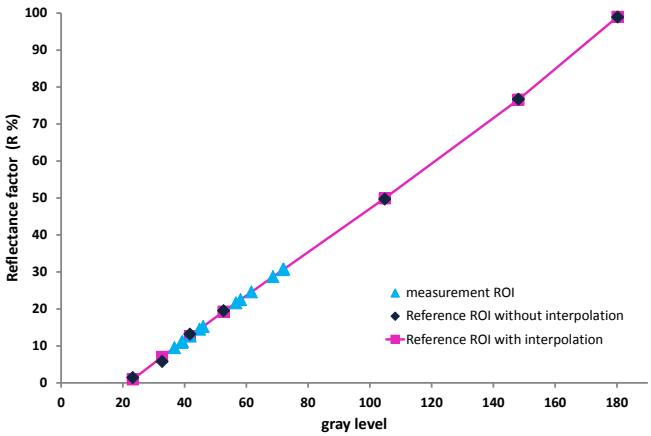

Fig. 2.11: Interpolation by third-degree polynomial (pink line) between gray levels and reflectance values of standards (blue dots). Measurement regions are indicated in pale blue.

2.3 Spectrophotometry by integrating sphere

Contact spectrophotometry is a non-destructive technique, requiring the contact with sample surface to perform measurements of small areas. For its accuracy and repeatability, due to the fixed measurement geometry, it is used as reference technique for IS reflectance spectra in the visible spectral range. Furthermore, reflectance data can be converted into colorimetric data for color difference evaluations.

Konica Minolta CM2600-d portable integrating sphere spectrophotometer is equipped by three pulsed xenon lamps (Fig. 2.12(a)); 1) for diffuse illumination, 2) for specular reflectance with ultraviolet component and 3) for emission without ultraviolet.

It makes possible to observe the areas of the specimen that we want to measure, thanks to an illumination LED system that turns on by opening the viewing port on the spectrophotometer (Fig. 2.12(a), 4).

Two different measurement apertures can be used, with 8 mm and 3 mm in effective diameter (Fig. 2.12(b), 2.12(c)).

These features allow to find the better area to measure. However the contact measurements require a sampling surface quite flat on which accommodate the instrument, the previous choice of sampling points and furthermore the investigated areas have point dimensions.

The IS survey has not these constraints, since large areas can be acquired, without contact with sample surface and the region of interests can be choose after the image acquisitions.

(a) (b) (c)

Fig. 2.12: Konica Minolta CM2600-d. (a) Illumination LED port (4); (b) Aperture mask of 3mm ∅; (c) Aperture mask of 8 mm ∅.

Integrating sphere (52 mm ∅), coated with *Spectralon*®, and the capture direction of diffuse radiation, determine a d/8 ° measurement configuration (Fig. 2.13).

In one measurement session the light sources flash sequentially. Specular component excluded data are calculated by software when the two light sources flashed: the light produced by the first xenon lamp is diffused inside the integrating sphere,

while the second light source reflects specularly the light from the specimen surface (Fig. 2.13(b)). In this way, the Specular Component Included (SCI) and Specular Component Excluded (SCE) data are obtained simultaneously from each measurement. By comparing such data the specular gloss feature of materials is calculated and may be omit.

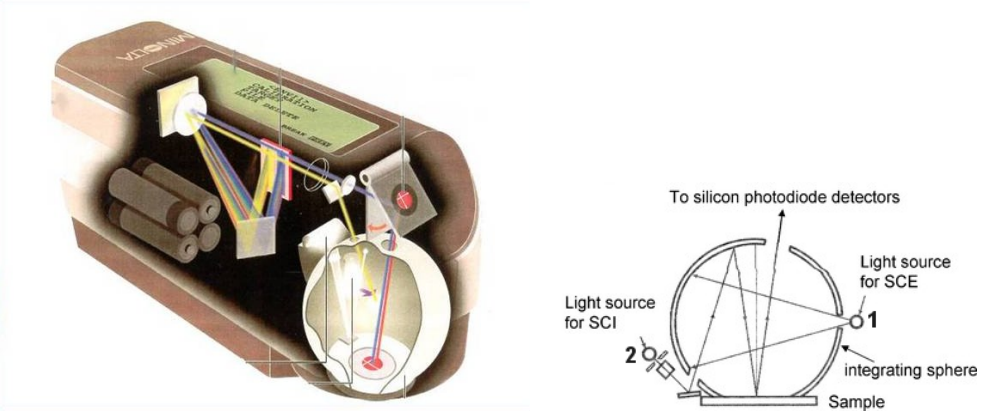

(a) (b)

Fig. 2.13: (a) Konica Minolta CM2600-d integrating sphere spectrophotometer and (b) its integrating sphere with d/8° measurement configuration.

Spectral reflectance data without UV component (0% UV) are obtained by using the third light source, fitted with UV 400 nm cutoff filter. By merging the spectral reflectance data obtained with and without UV component, the UV intensity correction is performed by software. Consequently, the eventual fluorescence emission of the investigated specimen can be excluded.

The light is divided in wavelength, from 360 to 740 nm with a 10 nm sampling pitch, by a holographic diffraction grating, before reaching the silicon photodiode array (Fig. 2.13(a)). Each sensor is sensitive to a particular wavelength.

Single measurement is the automatic averaging of three measurements. The systematic error is about 0.5; the estimated uncertainty on reproducibility on spectral data is approximately 0.28, while on colorimetric data is about 0.07.

The CM2600-d works with SpectraMagic NX software to obtain spectral and colorimetric measurements.

For the colorimetric data shown in this work, standard illuminant and observer used are respectively D65 and 10°, considering CIE 1964 color space. The measurement area is with 3 mm ∅.

2.4 Colorimetry

In this work, colorimetric investigations were carried out by using the *L*a*b* color space*, devised in 1976 as uniform space, unlike of the previous color spaces created by *CIE* (*Commission Internationale de l'Eclairage*, International Commission on illumination). The uniformity ensures that a change of the same amount in a color value should produce a change of the same visual importance in the CIELAB space. This model is suitable to investigate the color differences, which may represent the chromatic alterations of the art materials. It is represented by a three-dimensional model, in which the L* coordinate indicates the Lightness, that increases toward the top and decreases toward the bottom, while a* and b* are the chromaticity coordinates (Fig. 2.14). The saturation of the color increases moving out from the center [20].

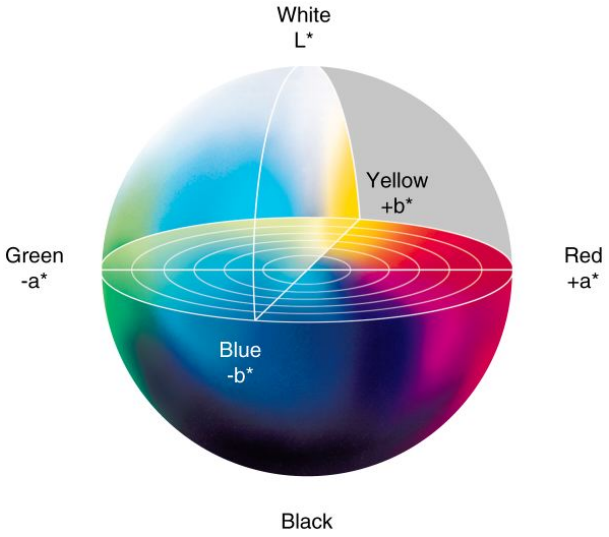

Fig. 2.14: CIELAB color space

In this diagram, +a* represents the red component, -a* represents the green component, +b* represents the yellow component, -b* represents the blue component.

They can be determined by taking into account the 10 ° *XYZ tristimulus values*, which are based on the *color matching functions* $\bar{x}_{10}$, $\bar{y}_{10}$, $\bar{z}_{10}$, defined in 1964 by CIE, in order to match to the sensivity of the human eye. By assuming a 10 ° Supplementary Standard Observer, the 10 ° *XYZ tristimulus values* are expressed by the following formulas:

$$X_{10} = K \int_{380}^{780} S(\lambda)\bar{x}_{10}(\lambda)R(\lambda)\, d\lambda$$

$$Y_{10} = K \int_{380}^{780} S(\lambda)\bar{y}_{10}(\lambda)R(\lambda)\, d\lambda$$

$$Z_{10} = K \int_{380}^{780} S(\lambda)\bar{z}_{10}(\lambda)R(\lambda)\,d\lambda$$

where:

$$K = \frac{100}{\int_{380}^{780} S(\lambda)\bar{y}_{10}(\lambda)\,d\lambda}$$

and
$S(\lambda)$ is the spectral power distribution of the illuminant;
$\bar{x}_{10}$, $\bar{y}_{10}$, $\bar{z}_{10}$ are the Color matching functions for 10 ° Supplementary Standard Observer;
$R(\lambda)$ is the spectral reflectance of the specimen.

From the equations above, it follows that:

$$L^* = 116(Y_{10}/Y_n)^{1/3} - 16$$

$$a^* = 500[(X_{10}/X_n)^{1/3} - (Y_{10}/Y_n)^{1/3}]$$

$$b^* = 200[(Y_{10}/Y_n)^{1/3} - (Z_{10}/Z_n)^{1/3}]$$

where:
X_{10}, Y_{10}, Z_{10} are tristimulus values, for 10 ° Supplementary Standard Observer, of the specimen.
X_n, Y_n, Z_n are tristimulus values, for 10 ° Supplementary Standard Observer, of a perfect reflecting diffuser.

The color difference, $\Delta E^*{}_{ab}$, indicated in Fig. 2.15, is an euclidean distance [24].

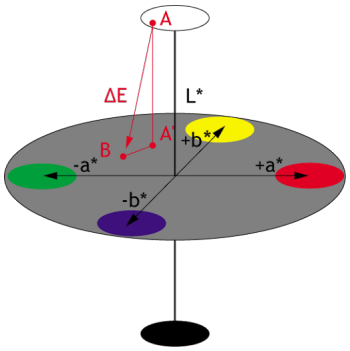

Fig. 2.15: Color difference $\Delta E^*{}_{ab}$ in CIELAB color space. A: Target color; B: Specimen color; A': Target color at the same lightness as specimen color.

By considering two different colors, it can be calculated according to the following equation:

$$\Delta E^*{}_{ab} = \sqrt{(\Delta L^*)^2 + (\Delta a^*)^2 + (\Delta b^*)^2}$$

The color difference ΔE^*_{ab} equal to unity is considered as the limit of color discrimination. The human eyes can perceive variations greater than this limit value.
Colorimetric analysis on art materials was performed by using the integrating sphere spectrophotometer, previously described. Such instrument calculates the tristimulus values X, Y, and Z by software, integrating the spectral reflectance data obtained on specimen. In this way, the spectrophotometer can be distinguished from a tristimulus instrument, since it calculates directly tristimulus values by using three sensors filtered to have the same sensibility of color-matching functions $\bar{x}$, $\bar{y}$, $\bar{z}$.

2.5 Principal component analysis (PCA)

The Principal Component Analysis (PCA) is a technique of multivariate statistics, widely used for simplification of complex data systems. The aim of this technique is the reduction of the number of variables through a linear transformation of the variables. In this new system, the variables are ordered in decreasing order of variance. This allows to represent the maximum variance of the system through the minimum number of principal components.

PCA was applied to reflectance spectral data obtained by IS inspections. From a system of fifteen variables, correspondent to the wavelengths, in most cases a system of two variables is derived. The higher sensitivity in detecting early signs of alteration on spectral data, makes the monitoring of artworks by IS more effective.

The PCA was carried out by using an MS Excel© add-in, XLSTAT2007[5], available on Windows platform.

2.5.1 Mathematical description

Each reflectance spectrum measured on N wavelengths is considered as a vector with N components. If M spectra have been measured, we get a matrix MxN of reflectance values (Table 2.2). Each row represents a single spectrum (generally called *sample* or *observation*). Each column collects the measurements at a single wavelength (called *variables*).
The measurement x_{ij} in the matrix is the reflectance measured at wavelength i ($i = 1, 2,..., N$) in the spectrum j ($j = 1, 2,..., M$). The mean value of the spectrum j is the following:

$$\mu_j = \frac{\sum_{i=1}^{N} x_{ij}}{N}$$

[5] XLSTAT2007 by Addindoft^{TM}

	410	450	490	514	570	612	649	690	710	730	790	850	910	970	1050
Lit_oil1	64	73.8	83.2	87	87.8	88.2	88.2	77.5	71	70.7	89	90.5	89.4	91.1	95.7
Lit_oil2	65	74.8	83.6	87.4	88.1	88.7	88.5	77.7	71.7	70.8	89.3	90.8	89.7	91.5	95.7
Lit_oil3	65.8	75.3	83.6	87.4	88.2	88.9	88.4	77	71.8	70.8	89.2	90.7	89.3	91	95.7
Lit_oil4	65.5	75	83.4	87.1	87.9	88.4	88.1	77.5	71	70.7	88.9	90.3	89	90.7	95.7
Lit_gl1	71	76	89.3	89.3	90.2	89.8	88	75.2	69.5	67.7	90.3	91.3	91.1	92.4	95.7
Lit_gl2	73	79.2	89.6	89.9	90.5	90.2	88.3	75	69	67	90.7	92	91.5	93	96.3
Lit_gl3	73.5	78	89.2	89.3	90.2	90	87.9	74	69	67.2	90.2	91.4	90.9	92.5	95.7
Lit_gl4	71	75	87.8	88	89.2	89.1	86.8	74	68.5	66	88.9	89.8	89.5	90.6	95.7

Table 2.2: Matrix 8 x 15 carried out with a data set of eight VIS-NIR reflectance spectra.

The *variance* of the same spectrum is defined as:

$$\sigma_j{}^2 = \frac{\sum_{i=1}^{N}(x_{ij} - \mu_j)^2}{N-1}$$

The *covariance* between the spectra 1 and 2 is:

$$\sigma_{12} = \frac{\sum_{i=1}^{N}(x_{i1} - \mu_1)(x_{i2} - \mu_2)}{N-1}$$

which is evidently identical to covariance between spectra 2 and 1:

$$\sigma_{12} = \sigma_{21}$$

Variance of a spectrum is then a peculiar case of covariance:

$$\sigma_{11} = \sigma_1^2$$

As result of these definitions, from the MxN matrix of observations, a symmetrical square *covariance matrix* cov(x) is obtained (Table 2.3) [23].

This matrix, due to its symmetry, may be diagonalized, leading to:

$$\begin{bmatrix} \lambda_1 & 0 & 0 & \dots \\ 0 & \lambda_2 & 0 & \dots \\ 0 & 0 & \lambda_3 & \dots \\ \vdots & \vdots & \vdots & \ddots \end{bmatrix}$$

PCA consists in this diagonalization.

The PCA searches the best-fitting set of orthogonal axis of the new space, in which replace the initially-given set of data. The simplest way is by finding the projections on the new axis which maximize the variance. The first principal component is the direction in the new space along which projections have the largest variance. The second principal component is the direction which maximizes variance among all directions orthogonal to the first. Likewise the other principal components are found [18].

Variables	410	450	490	514	570	612	649	690	710	730	790	850	910	970	1050
410	**15.209**	5.854	11.437	4.154	4.321	2.749	-0.886	-5.913	-4.709	-7.507	2.130	1.461	3.050	2.460	0.377
450	5.854	**3.273**	4.233	1.868	1.770	1.239	0.080	-1.822	-1.433	-2.283	1.149	1.045	1.474	1.403	0.284
490	11.437	4.233	**9.013**	3.288	3.406	2.118	-0.632	-4.400	-3.610	-5.748	1.739	1.198	2.515	2.026	0.290
514	4.154	1.868	3.288	**1.325**	1.309	0.853	-0.061	-1.428	-1.159	-1.861	0.783	0.636	1.069	0.943	0.148
570	4.321	1.770	3.406	1.309	**1.324**	0.848	-0.148	-1.577	-1.270	-2.039	0.736	0.558	1.028	0.871	0.128
612	2.749	1.239	2.118	0.853	0.848	**0.568**	-0.043	-0.962	-0.726	-1.209	0.498	0.404	0.672	0.593	0.089
649	-0.886	0.080	-0.632	-0.061	-0.148	-0.043	**0.285**	0.572	0.490	0.762	0.088	0.191	0.043	0.150	0.024
690	-5.913	-1.822	-4.400	-1.428	-1.577	-0.962	0.572	**2.576**	2.016	3.227	-0.618	-0.299	-0.969	-0.673	-0.085
710	-4.709	-1.433	-3.610	-1.159	-1.270	-0.726	0.490	2.016	**1.764**	2.694	-0.496	-0.229	-0.806	-0.550	-0.102
730	-7.507	-2.283	-5.748	-1.861	-2.039	-1.209	0.762	3.227	2.694	**4.291**	-0.800	-0.374	-1.288	-0.871	-0.160
790	2.130	1.149	1.739	0.783	0.736	0.498	0.088	-0.618	-0.496	-0.800	**0.520**	0.474	0.679	0.649	0.097
850	1.461	1.045	1.198	0.636	0.558	0.404	0.191	-0.299	-0.229	-0.374	0.474	**0.483**	0.589	0.611	0.099
910	3.050	1.474	2.515	1.069	1.028	0.672	0.043	-0.969	-0.806	-1.288	0.679	0.589	**0.920**	0.849	0.124
970	2.460	1.403	2.026	0.943	0.871	0.593	0.150	-0.673	-0.550	-0.871	0.649	0.611	0.849	**0.834**	0.120
1050	0.377	0.284	0.290	0.148	0.128	0.089	0.024	-0.085	-0.102	-0.160	0.097	0.099	0.124	0.120	**0.045**

Table 2.3: Covariance matrix obtained on Lithopone data set (Chapter 4.2).

The other method that is equivalent to maximizing the variance is to search the projections with the smallest average (mean-squared) distance between the original vectors and their projections on the principal components.

By assuming that the matrix X is centered, so that the mean of the vectors is zero, we have that the *variance* is:

$$\sigma_{\overrightarrow{p_i}}{}^2 = \frac{\sum_{i=1}^{N}(x_i \cdot p_i)^2}{N-1}$$

where p is the vector, so that maximize the variance $\sigma^2_{\overrightarrow{p_i}}$. With such purpose we constraint its maximization according to which it must have unit length, thus is $\overrightarrow{p_i}\,\overrightarrow{p_i} = 1 (or\ p_i^\intercal p_i = 1)$. Furthermore, if the summation is replaced by the MxN matrix, X, the projections in the new space are given by Xp_i, which correspond to Mx1 matrix. It follows that:

$$= \frac{(Xp_i)^\intercal (Xp_i)}{N-1}$$

$$= p_i^\intercal \frac{X^\intercal X}{N-1} p_i$$

$$= p_i^\intercal cov(X) p_i$$

In order to maximize this last function and the variance $\sigma^2_{\overrightarrow{p_i}}$, the Lagrange multiplier λ is introduced in the equation:

$$p_i^\intercal cov(X) p_i - \lambda(p_i^\intercal p_i - 1)$$

By setting the derivative of the Lagrangian equal to zero, it is:

$$cov(X) p_i = \lambda_i p_i$$

in which p_i are the *eigenvectors* associated at λ_i *eigenvalues* of matrix X [30].

For the covariance matrix, the eigenvectors p_i correspond to principal components and the eigenvalues λ_i to the variance explained by the principal components. The eigenvectors p_i are arranged in decreasing order of corresponding eigenvalues. Therefore the first principal component, corresponding to the eigenvector p_1 which goes the largest value of eigenvalue, λ_1, is the direction of maximum variance. The second principal component, corresponding to the eigenvector p_2 is the direction orthogonal at the first component and with the most variance, and so on for the next principal components. Eigenvectors are uncorrelated with each other, because they are orthogonal between them. The eigenvalues describe the total variance of each component [30]. This is showed in Fig. 2.16.

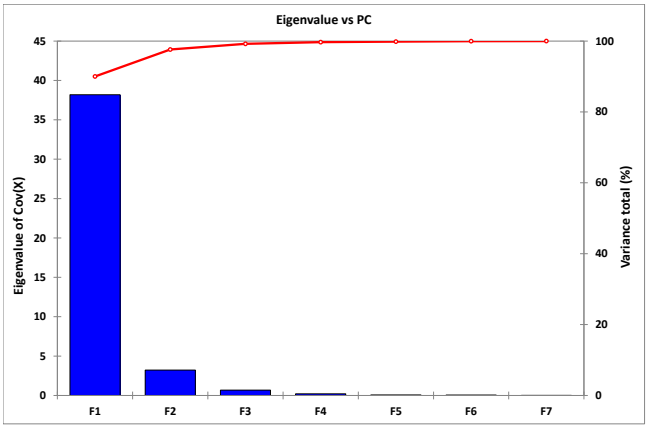

Fig. 2.16: Eigenvalues of covariance matrix are in relation to principal components and to the captured variance. The 90% of variance is represented by the first PC. By considering also the second PC the cumulative variance rises up to 98%. Thus, almost all the information is enclosed in the first two PCs.

The results of PCA are usually showed in terms of components *scores* t_i and *loadings* p_i.

The *scores* are the transformed variable value corresponding to a particular data point and represents the row vectors t_i with respect to principal components. The *loadings* are the weight by which each original variable should be multiplied to get the component score and represents the column vectors p_i of cov(X) matrix.

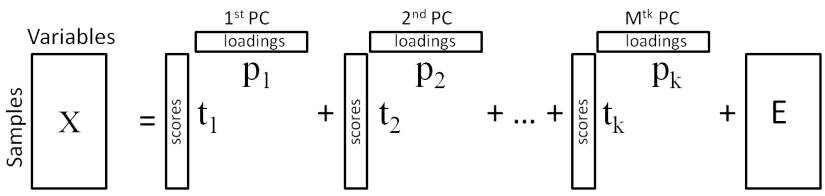

$$X = t_1 p_1{}^{\intercal} + t_2 p_2{}^{\intercal} + ... + t_k p_k{}^{\intercal} + ... + t_q p_q{}^{\intercal} + E$$

where:
t_i are the *scores* vectors;
p_i are the *loadings* vectors;
k =number of Principal Component (PC) or *factors*;
$q \leq (m, n)$;
E is the residual matrix, constituted of the PCs with small variance.

The *scores* and the *loadings* are ordered by amount of variance captured in descending order.

The *scores* form an orthogonal set, T_k matrix, that describes the relationship between *samples*.

The *loadings* form an orthogonal set, P_k matrix, that describes the relationship between *variables* [40]. The loadings allow to estimate the weight of a variable with respect to a defined principal component. Each variable has a loading value for each component (Fig. 2.17). In this example, it is evident that the variables 410 and 490 contribute strongly to the first PC. The variables 690, 710 and 730 weigh negatively on first PC, since they show distinct features than other variables. The other variables contribute differently to the second PC, although we have a slight weight also on the first.

Furthermore, loadings and scores can be plotted in pairs in biplot graph in order to investigate the correlation among samples and the relationship between variables, as showed in Fig. 2.18.

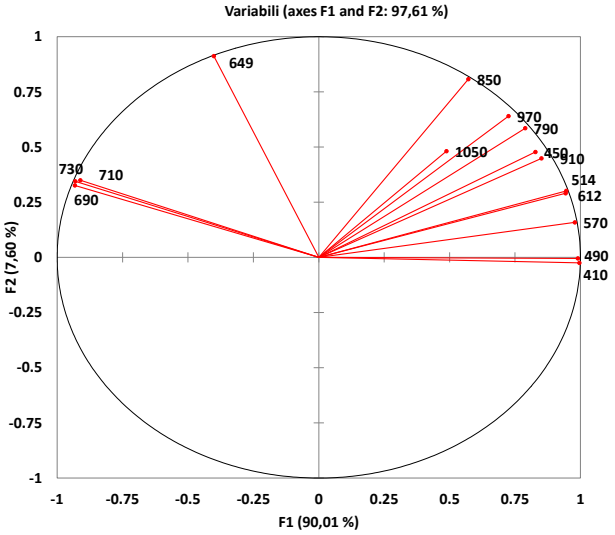

Fig. 2.17: Loading graph. It is clear in this instance that 410 and 490 nm wavelengths are responsible for the separation.

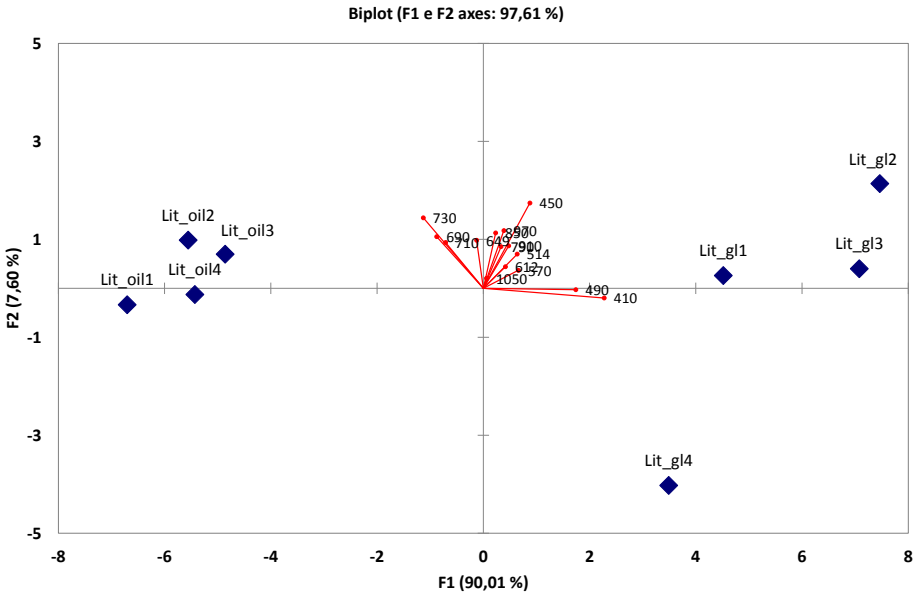

Fig. 2.18: Biplot graph of loading and score vectors of covariance matrix.

Chapter 3

Image spectroscopy device

In the first phase of this work, I focalized my attention on the multispectral device. The goal was improving quality of the acquired images, at the wavelengths where silicon CCD has low sensibility and at the same time, reducing errors in the reflectance spectral factor due to the method.

3.1 Spectral filtering

3.1.1 Test bench

Several optical filtering systems have been tested to sample the VIS-NIR range by IS. Measurement of the transmitted band was carried out by the apparatus shown in Fig. 3.1. The radiation outgoing from a tungsten halogen lamp, by means of an optical fiber reaches a grating monochromator, selecting wavelengths. Light of the selected band is then collected by a second optical fiber and diffused in front of the IS device[1] through the use of clear adhesive tape. Measurements are performed on the image (Fig. 3.2), summing up the gray level output on the light spot.

This simple test bench is not meant to perform absolute measurements, but rather to assess the consistency of the IS device. Indeed, provided that no saturation is reached in the images, any measurements is mediated by the sensitivity of the CCD employed (Fig. 3.3).

3.1.2 Edgepass combinations

The original aim of the double-wheel filter changer was to cover continuously the VIS-NIR range, 400 - 1000 nm, with high luminosity on the detector and even

[1]The tungsten halogen lamp, optical fibers, and the scanning monochromator *MonoScan-2000*, covering spectral range of 300-1050 nm, 4 nm spectral resolution, by Ocean Optics, USA.

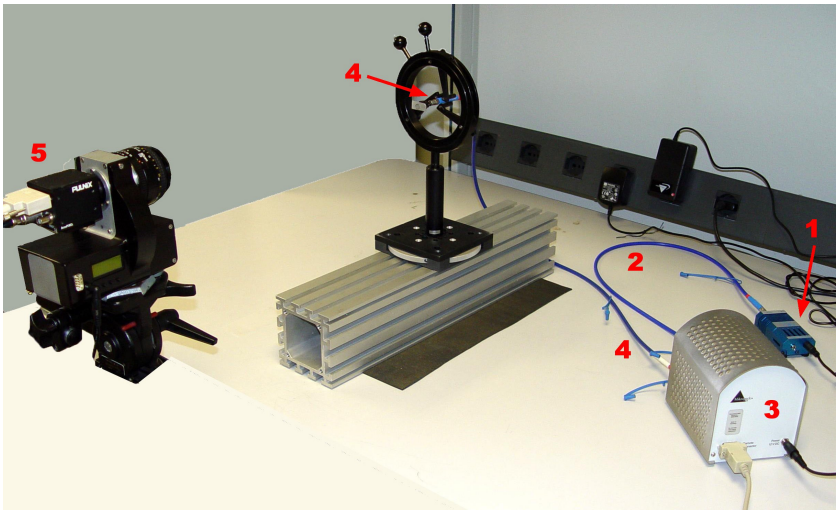

Fig. 3.1: Optical bench used for measurements on transmission of interferential filters: light source (1), optical fibers (2, 4), monochromator (3), Pulnix TM1325-CL camera fitted with filters (5).

possibility to select the bandwidth. Long pass and short pass filters[2] in the spectral range from 500 nm up to 850 nm are taken into account. They are interferential filters, which should provide a sharp cut-off either above or below a particular wavelength.

A set of 8 long-pass filters cover the VIS-NIR spectral range, transmitting the radiation at wavelengths longer than 500 nm (Fig. 3.4). Short pass filters cover the 400 - 850 nm spectral range (Fig. 3.5). By using short-pass and long-pass filters, seven filter combinations with a bandwidth of 50 nm are obtained. The results achieved on their transmitted bands are shown in Fig. 3.6.

The characterization of these filters, performed in the spectral range between 400 and 970 nm, has revealed that the rejection band for the short pass filters of 500 nm, 550 nm and 600 nm, is limited to 750 nm (Fig. 3.5). As a result, in the first two combinations (Fig. 3.6(a), 3.6(b)), there is up to 20% of transmitted radiation even at longer wavelengths than the allowed band.

This constitutes a serious drawback for the system, because it requires a supplementary absorption filter, giving some problems to the hardware setup. Moreover, significant variations of the detector sensitivity, particularly at 673, 721, 767, 820 nm, are shown. The filter bandwidth of 50 nm seems to be affected significantly by these changes in sensitivity. Then, any reflectance measurements in these bands will be in fact a weighted mean of both reflectance and CCD sensitivity, which gives little guarantee of repeatability.

[2]Edgepass filters by Thorlabs Inc., Newton, New Jersey, USA. Long pass filters are constituted by the FEL0500 - FEL0850 series, while short pass filters are constituted by the FES0500 - FES0850 series.

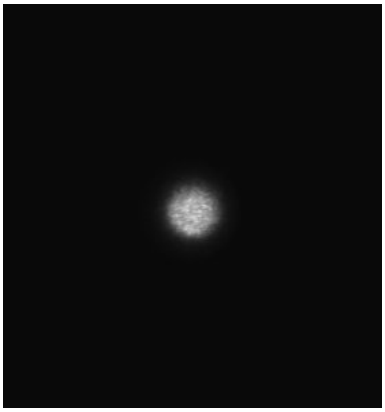

Fig. 3.2: Light spot produced by a filter combination and detected by IS device.

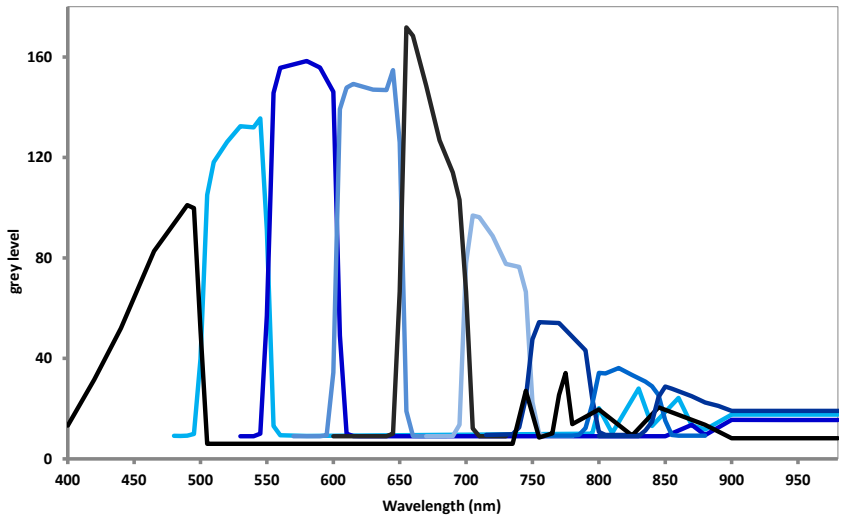

Fig. 3.3: Spectral bands covered by edgepass set of filters, used for IS analysis.

Applications and results

To verify the efficiency of such set of filters for IS, an investigation on white and blue layers of a painting on wood is performed (Fig. 3.7). The VIS-NIR reflectance spectra derived by multispectral images (Fig. 3.8) do not exhibit the expected results in terms of accuracy in deriving the reflectance values and of consistency with the spectra obtained by contact measurements (Fig. 3.9). By comparing of the the data obtained with the distinct tecniques, it can be claimed that the maximum value of $\Delta R\%$ are 5.7 for W1 sampling point, 2.5 for W2 point and 12.9 in the case of blue point.

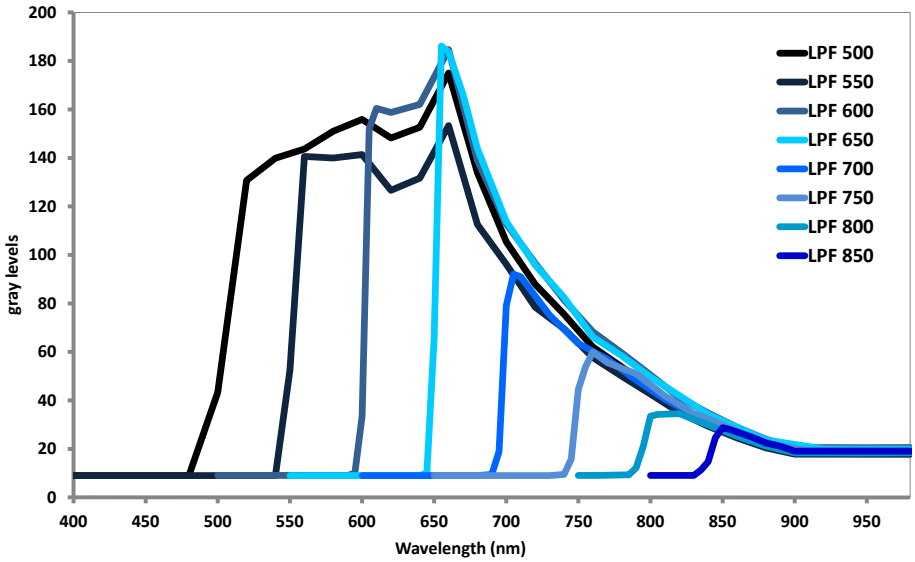

Fig. 3.4: Set of the characterized long-pass filters (LPFs).

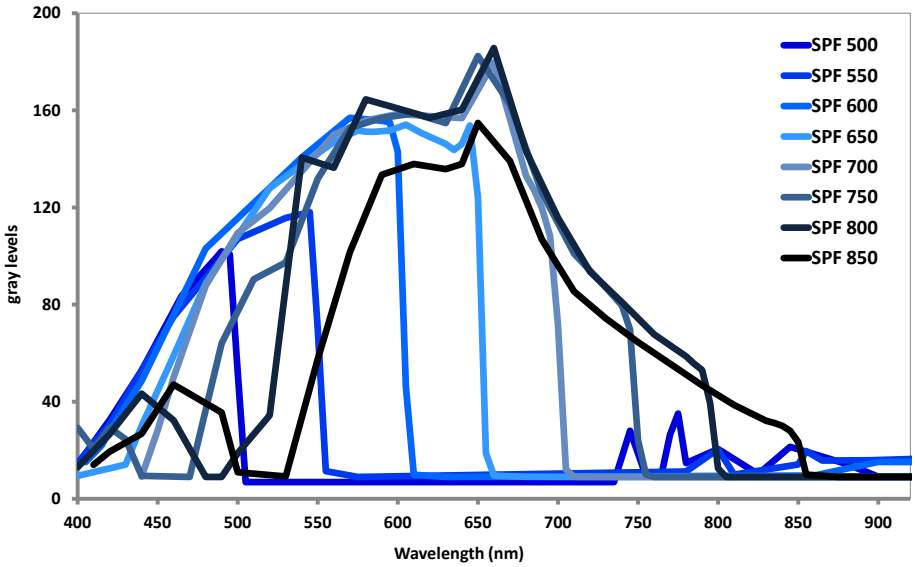

Fig. 3.5: Set of the characterized short-pass filters (SPFs).

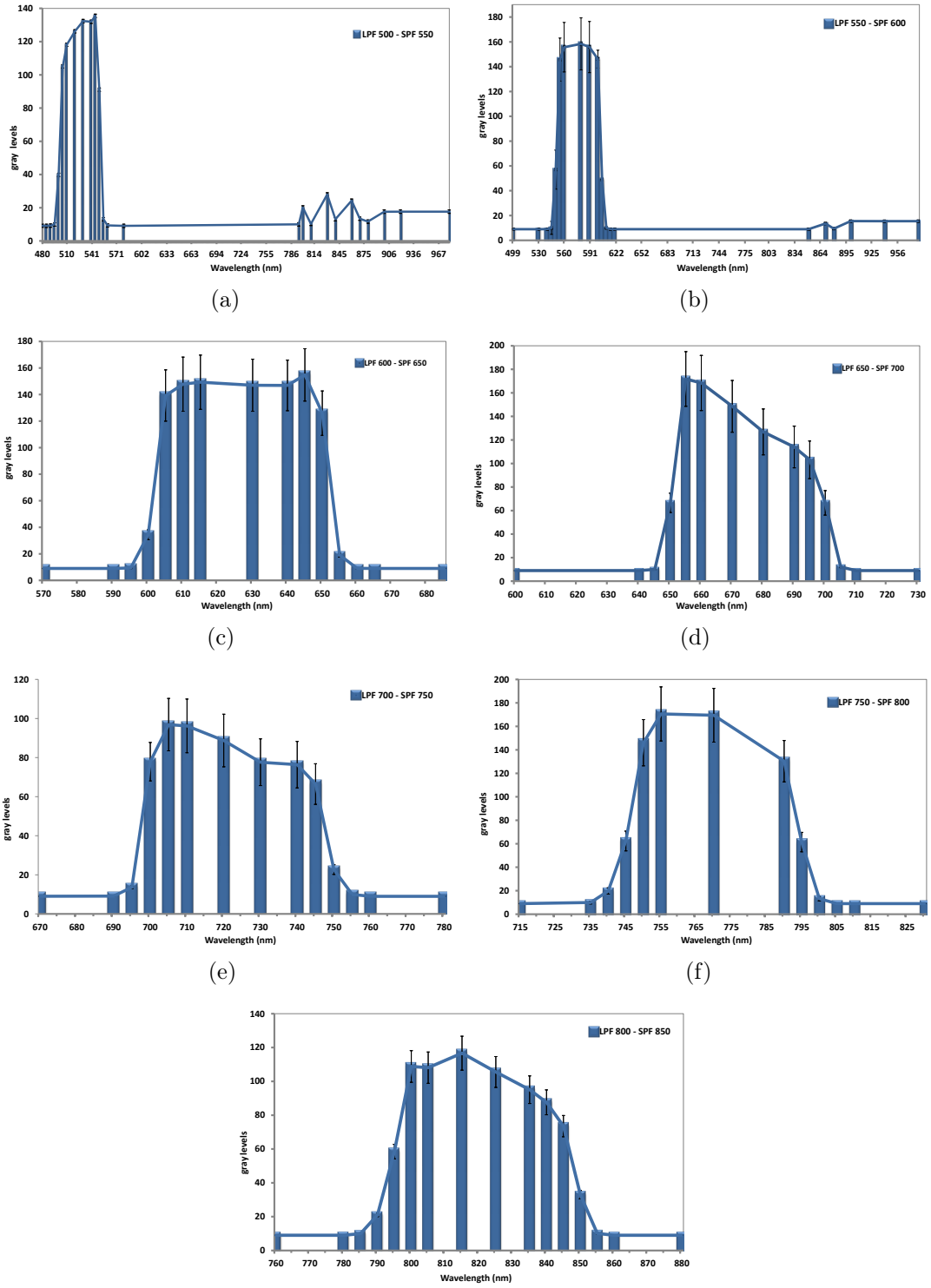

Fig. 3.6: Combination set of filters with 50 nm bandwidth. Bin width is representing the spectral resolution (4 nm) of the monochromator. It is simply shown the spectral range in which transmission bands were detected.

Fig. 3.7: *Country house*, XX century, oil on wood panel, private collection.

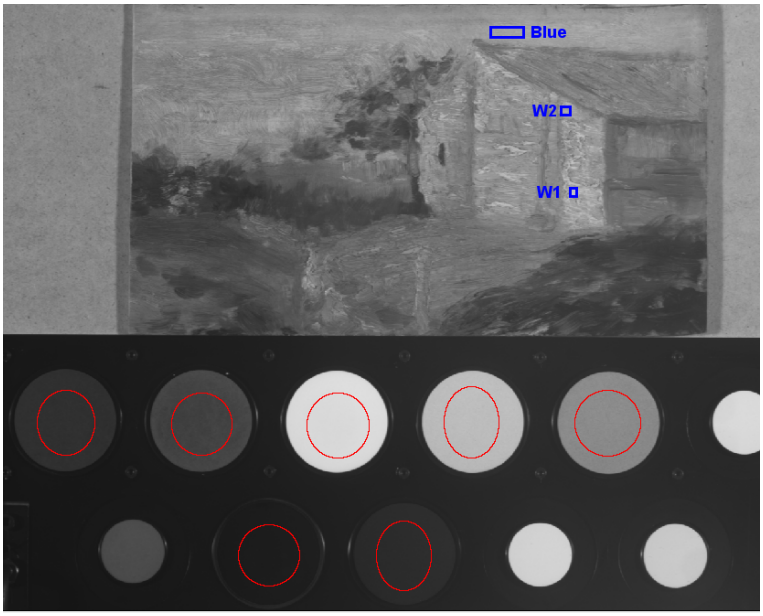

Fig. 3.8: *Country house*. Image captured by IS at 721 nm. Measurements ROIs on blue and white areas.

3.1.3 Narrow-band filters

For the reasons described above, it was decided to replace the edgepass filters with narrow bandpass filters, 10 nm FWHM bandwidth[3].

Both problems remarked with the edgepass filters have been solved. The IR stray light is absorbed by the substrate of the filters themselves. The sensitivity of CCD is steady enough in 10 nm bands. Measurements of some narrow bandpass filters have been carried out and the results are shown in Fig. 3.10. The plotted curves of transmitted light have been fitted by a Gaussian function.

Application and results

The narrow passband filters are tested by performing an investigation by IS on two different typologies of test objects[4], realized on canvas, 10 x 10 cm, and by using vinylic binder. The first one is divided in five sections, made by adding a further layer of the same pigment (Fig. 3.11(a)). The second test object is characterized by two distinct pigments, overlapping in the central portion of canvas (Fig. 3.11(b)).

The IS analysis concerns the following layers (Fig. 3.12): Naples Yellow ($Pb_2Sb_2O_7$), Deep cobalt green ($CoCr_2O_4$), Chromium oxide green - opaque (Cr_2O_3) and the last one, related to the second type of test object, Naples Yellow + Lead white ($2\,PbCO_3{\cdot}Pb(OH)_2$).

The results are compared with data achieved on the same sampling points through contact spectrophotometric measurements, with the aim to attest their reliability.

It can be generally argued that the spectra of the different pigment layers match the related reference spectra satisfactorily. Only the Naples Yellow (Fig. 3.13(a)) shows a wider margin of error, $\Delta R\% \cong 4.41$, at higher reflectance values, while in the case of Yellow Naples with Lead White the maximum value of $\Delta R\%$ is 2.0. The Chromium oxide green - opaque shows a $\Delta R\%_{max} \cong 2.02$ at 410 nm, while for Deep cobalt green the reflectance values of IS spectrum reach 1.55% of deviation at 650 nm. In any case spectra are reasonably well described by image-derived spectra.

[3]Bandpass filters by Thorlabs Inc., Newton, New Jersey, USA.

[4]The test objects were realized by the *Cultural Heritage Restoration and Conservation Center "La Venaria Reale"*, realised, in Turin, Italy.

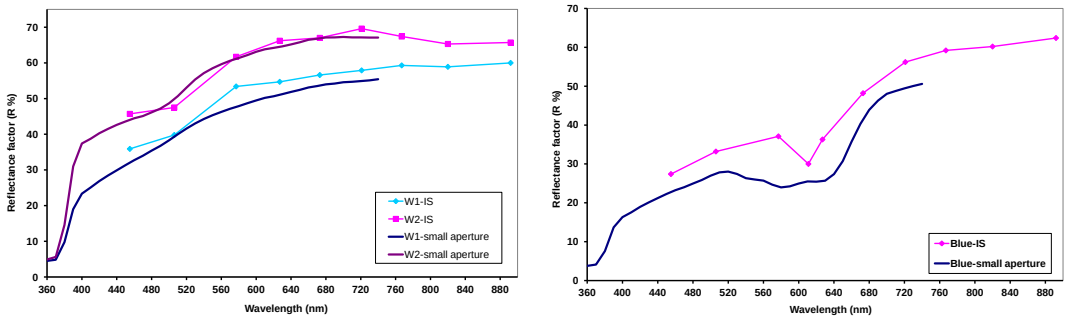

(a) (b)

Fig. 3.9: VIS-NIR reflectance spectra of (a) white ROIs and (b) blue ROI, compared to spectra achieved by contact spectrophotometer.

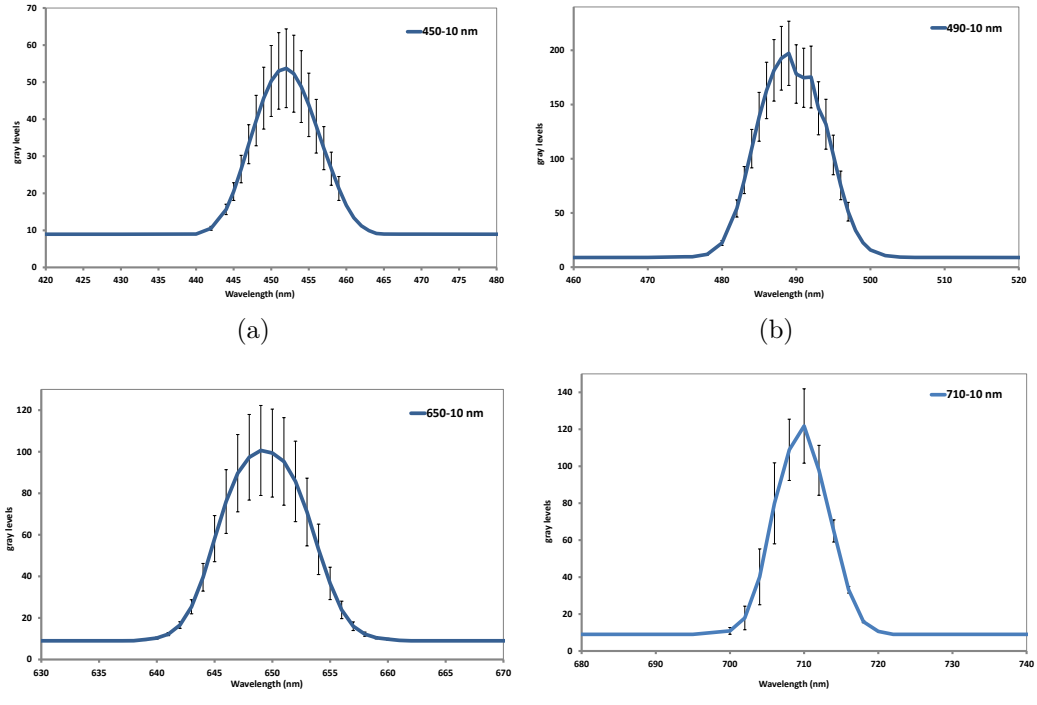

(a) (b)

(c) (d)

Fig. 3.10: Some characterized filters, 10 nm bandwidth.

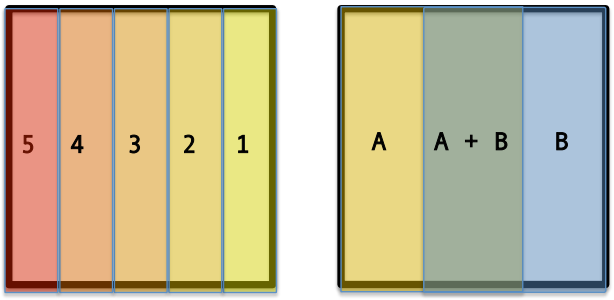

(a) (b)

Fig. 3.11: Representation of the two typologies of test objects used.

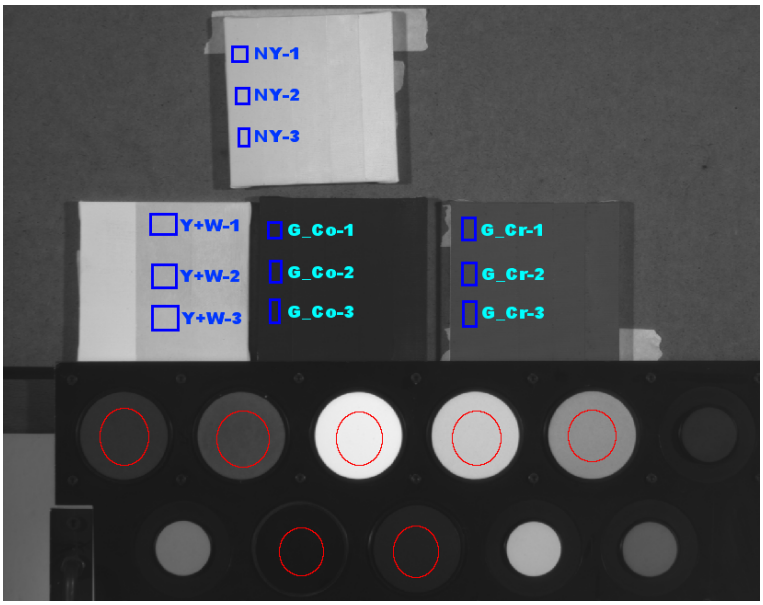

Fig. 3.12: Test objects, in counterclockwise order: Naples Yellow, Naples Yellow + Lead white, Deep cobalt green and Chromium oxide green - opaque layers. Image collected by IS at 530 nm.

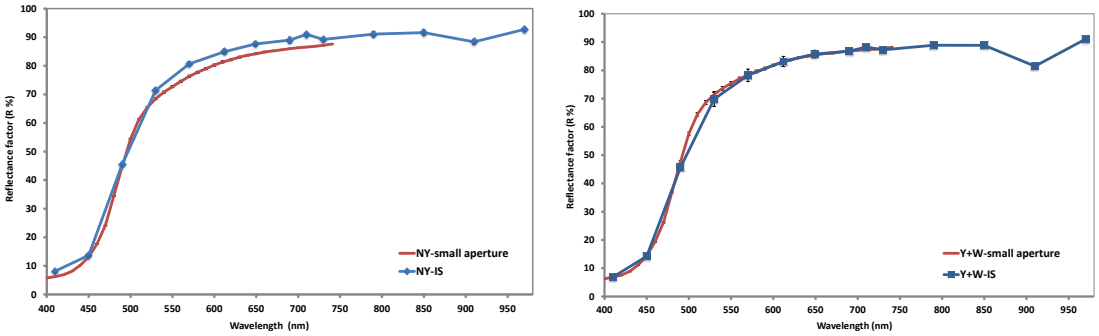

(a) (b)

Fig. 3.13: Mean VIS-NIR reflectance spectra obtained by IS, compared to spectra achieved by small aperture spectrophotometer. (a) Naples Yellow (b) Naples Yellow + Lead white.

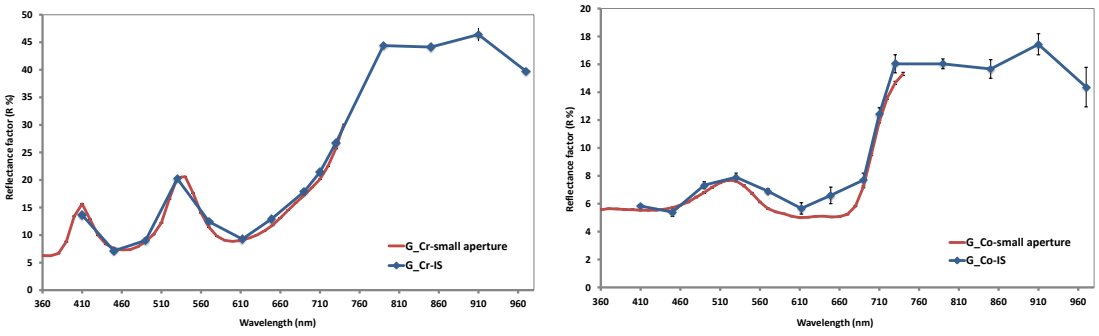

(a) (b)

Fig. 3.14: Mean VIS-NIR reflectance spectra obtained by IS, compared to spectra achieved by small aperture spectrophotometer. (a) Chromium oxide green - opaque (b) Deep cobalt green.

Chapter 4

Applications

4.1 Tests on modern painting materials

The contemporary painting materials, as well as traditional materials, are subject to deterioration. But, differing from ancient pigments, no or little knowledge has been collected on their evolution. Their degradation can manifest as a chromatic alteration and, over time, can influence and affect the proper reading of the work.

The aim of this study is to put in evidence the small changes, almost imperceptible to the eye, in order to perform an early evaluation of the chromatic toning of these materials.

A technique and a method of statistical analysis, IS+PCA, have been developed to recognize the weakest chromatic alterations [3]. PCA is used on spectral data obtained by IS images in the VIS-NIR spectral range.

Colorimetry may be used subsequently to supplement the information collected through PCA for the identification of alteration trends [2].

Such study was made by using a test panel, prepared in 1997 with some modern painting materials (pigments, binders and varnishes), subject to artificial aging (Fig. 4.1).

Description and treatment of test panel

The test panel consists of three pigment painted layers, as Titanium White, Artificial Ultramarine Blue and Sienna Earth. Each pigment has been mixed with three different binders: acrylic resin, alkyd resin and linseed oil. Each pigment/binder pair is present in six frames, covered by six different varnishes on their right half (Fig. 4.1).

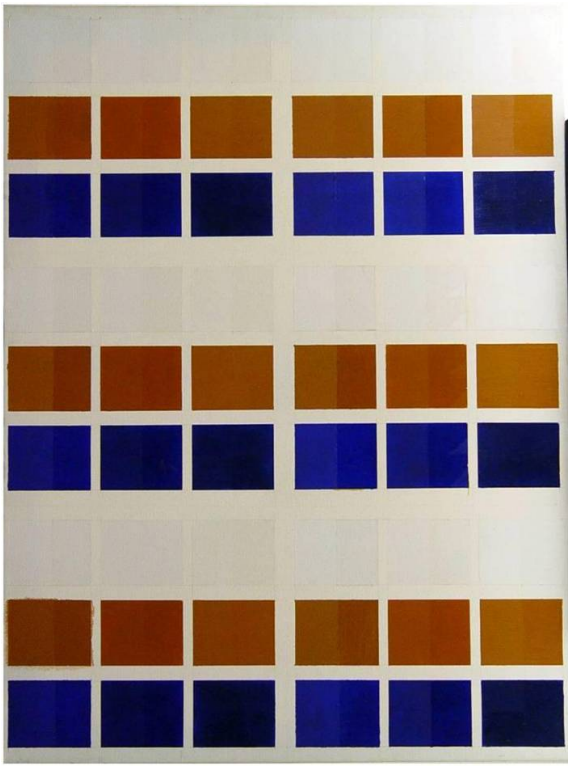

(a)

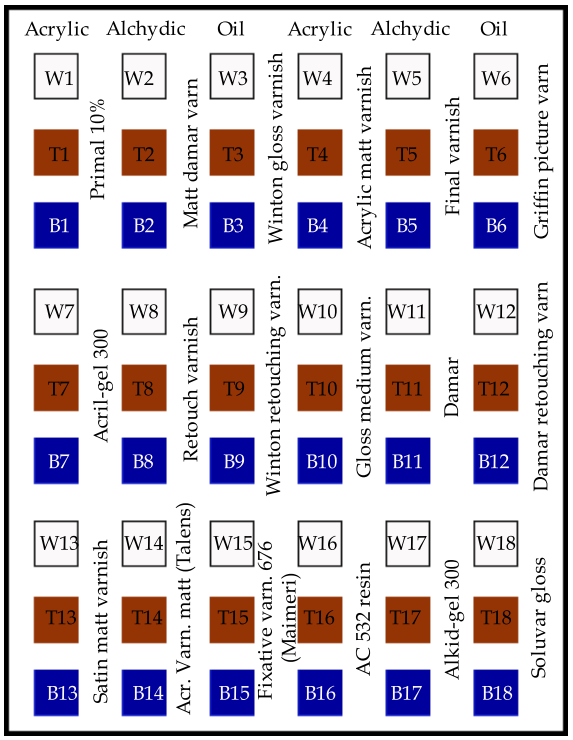

(b)

Fig. 4.1: (a) Test panel with Titanium White, Artificial Ultramarine Blue and Sienna Earth layers and (b) its schematic representation in which the names of the varnishes are reported.

The test panel was subjected to artificial aging by UV-VIS-IR irradiation with a 650 W sun lamp at a distance of one meter, for about eight-hours a day, for 376 hours total. The radiance illuminance produced by such lamp in the visible range is about 465 lux. The test panel underwent also to infrared irradiation for 259 hours by two 150 W IR-lamps. Each frame in the panel has been partly protected against irradiation, covering the upper part by a cardboard sheet. By this empirical aging procedure a wide range of cases is created, therefore, the possibility to evaluate the behavior of such materials in different situations (Fig. 4.2). We have focused on the non-varnished part. The image sequence of test panel, acquired at fifteen spectral bands is shown in Fig. 4.3.

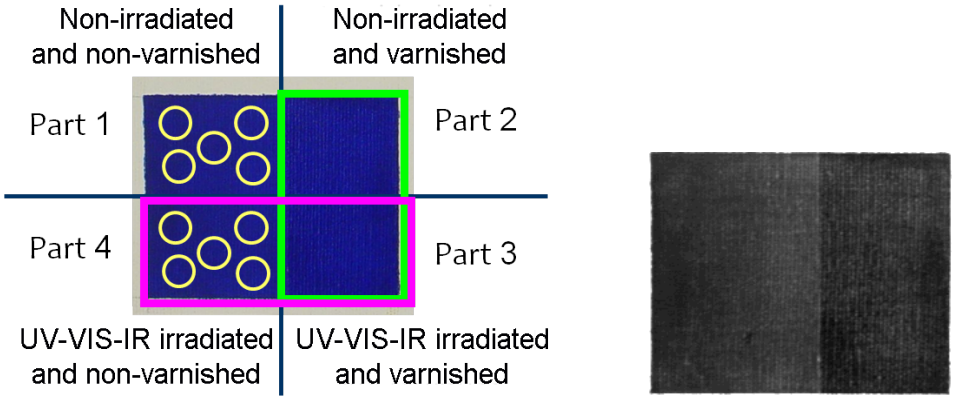

Fig. 4.2: Frame B13 of test panel. (a) Graphical representation of different treatments applied on each frame and of sampling points. (b) Image of the same frame collected at 710 nm by IS, in which is visible the difference between varnished and non-varnished part.

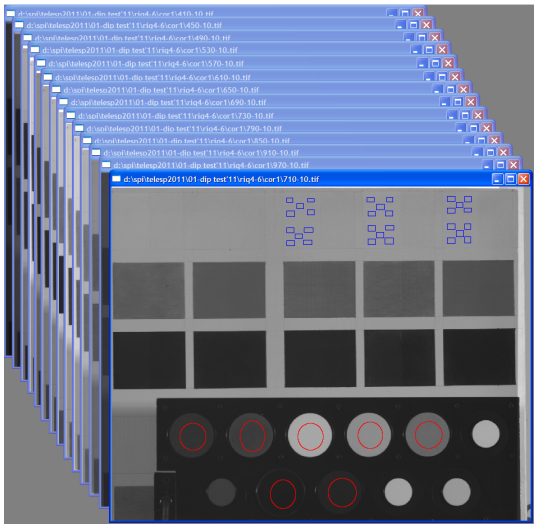

Fig. 4.3: Vis-NIR image cube of several frames of test panel.

4.1.1 Ultraviolet fluorescence survey

The UV fluorescence image (Fig. 4.4) shows that the varnished parts of each frames are the most fluorescent. Moreover, irradiated and non-irradiated parts are often well recognizable. It can be argued that the UV fluorescence capability mostly of varnishes is sensitive to previous irradiation.

Likewise, the binders show different fluorescence and linseed oil appears as the most fluorescent.

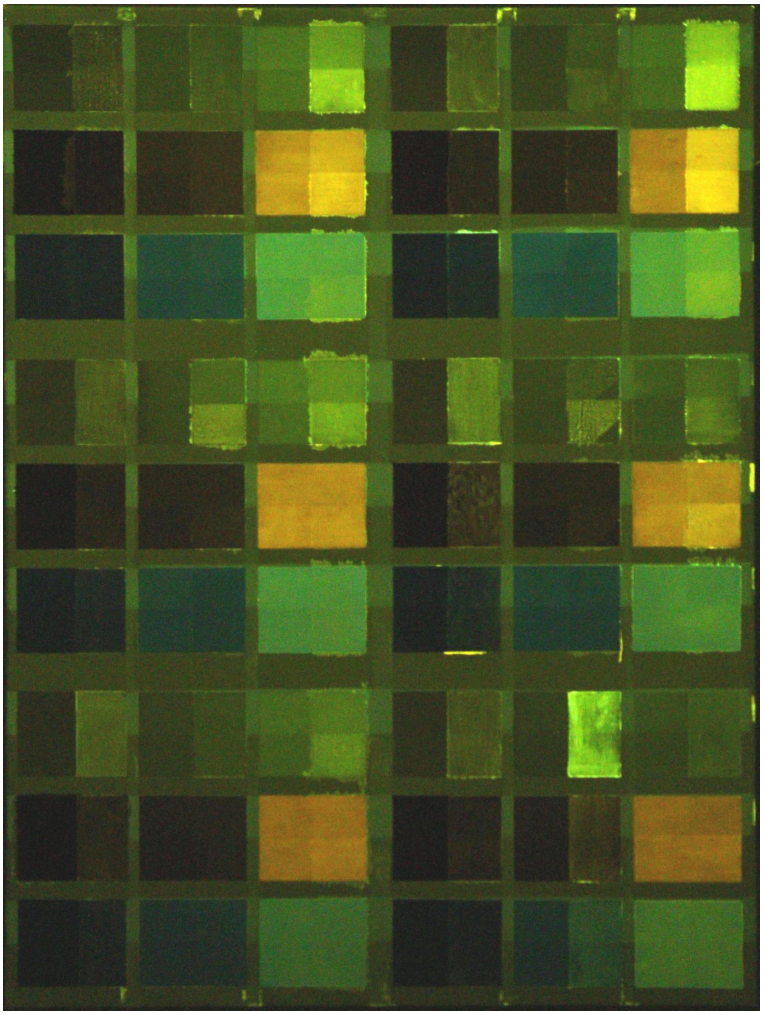

Fig. 4.4: Ultraviolet fluorescence image of test panel.

4.1.2 Test method: Discrimination of binders

As first test of the method, the capability of IS+PCA combination to discriminate between the three binders was evaluated.

These results are compared with colorimetric outcomes obtained by contact spectrophotometer on the non-varnished portions of frames. IS measurements were limited to the visible portion of the spectrum.

On Titanium White layers (Fig. 4.5(a)) the color appearance is very similar for all sampled points. The acrylic resin shows a separation from other media due to the b* parameter ($\Delta b^* \cong 1$), while a minor spread in a* is needed to separate alkyd sampling points from the others ($\Delta a^* \cong 0.2$).

In the PCA language, oil is well discriminated on the first PC, while acrylic and alkyd are separated on the second PC.

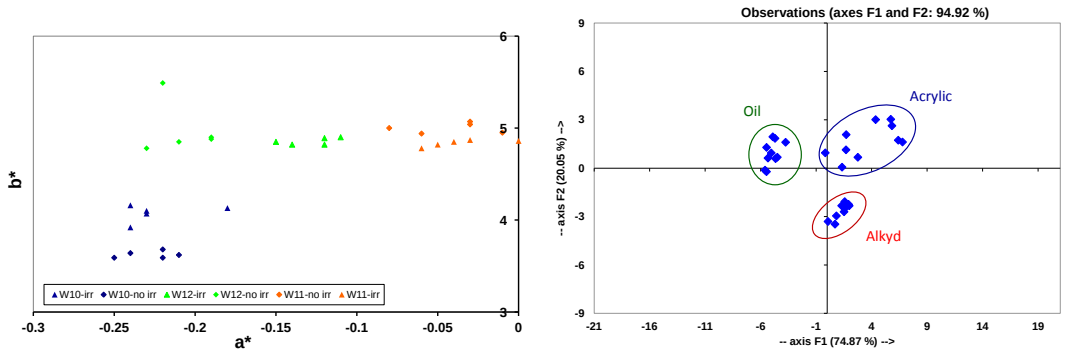

(a) (b)

Fig. 4.5: (a) Colorimetric results, a* and b*, on Titanium White in acrylic (blue), alkyd (red) and oil (green) binders. (b) Equivalent results obtained with PCA applied on IS data of the same layers of test panel.

For Sienna Earth layers (Fig. 4.6(a)), a wider spread in a* and b* values ($\Delta a^* \cong 5$, $\Delta b^* \cong 6$) is disclosed.

Concerning the Artificial Ultramarine Blue layers (Fig. 4.7(a)), the colorimetric data point out a significant differentiation between binders, determined mainly by the noticeable yellowish appearance of the oil layers ($\Delta b^* \cong 20$).

In the PCA application oil and acrylic media are well differentiated: they always show a separation on the first component. Similarly, the second component is needed to discriminate the alkyd binder.

Colorimetry and multivariate analysis, even with different languages, perform a good discrimination among binders. IS+PCA method performs a detailed discrimination even when the colorimetric parameters are well below the sensitivity of human eye (Fig. 4.5).

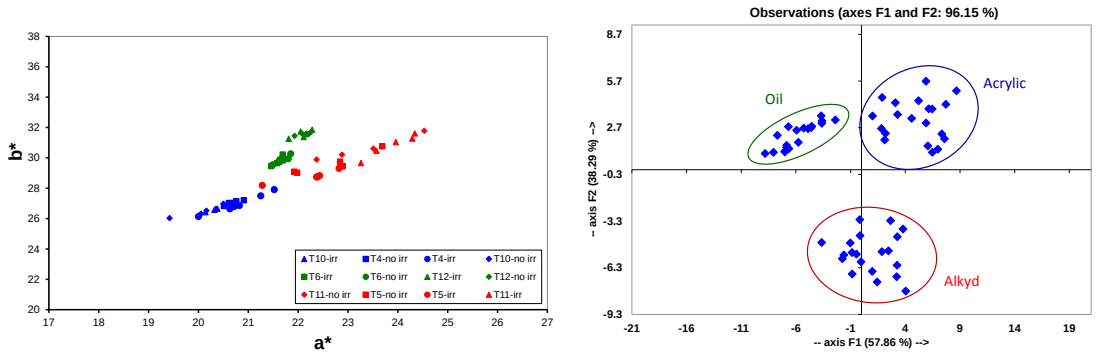

(a) (b)

Fig. 4.6: (a) Colorimetric results, a* and b*, on Sienna Earth in acrylic (blue), alkyd (red) and oil (green) binders. (b) Equivalent results obtained with PCA applied on IS data of the same layers of test panel.

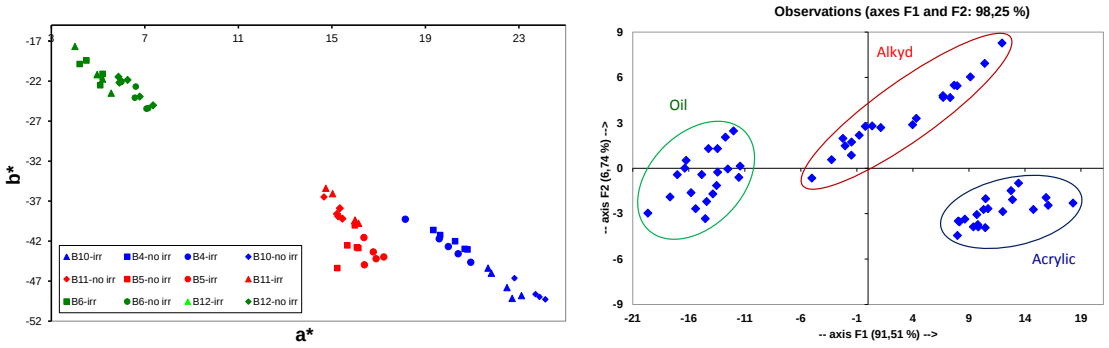

(a) (b)

Fig. 4.7: (a) Colorimetric results, a* and b*, on Artificial Ultramarine Blue in acrylic (blue), alkyd (red) and oil (green) binders. (b) Equivalent results obtained with PCA applied on IS data of the same layers of test panel.

4.1.3 Intrinsic variability of painted layers in acrylic binder

Due to its sensitivity, IS+PCA method may detect differences also in painting layers created by the same procedure.

A test of the intrinsic variability of hand-made color layers has been made, measuring by contact spectrophotometer the six frames of Titanium White with acrylic binder.

A sharp separation on first PC is apparent for frames W10, W16 against the others (Fig. 4.8(b)). A similar plot, limited to frames W10, W16 against W4 was obtained in old measurements (Fig. 4.8(a)). For some reasons, frames W10 and W16 were made different, even by the same manual procedure.

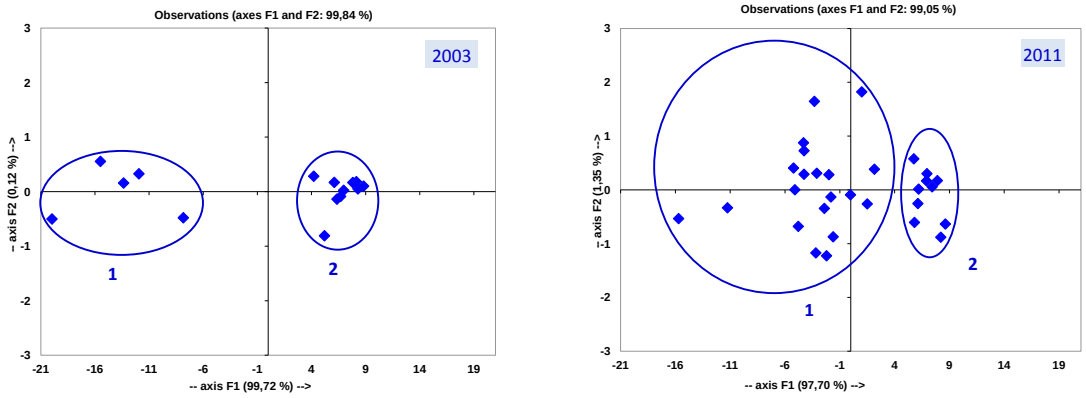

(a) (b)

Fig. 4.8: White frames in acrylic binder, non-irradiated portions, to test their intrinsic variability. (a) PCA results on W4 (1), W10 and W16 (2) - measurements 2003 (b) PCA results on W1, W4, W7, W13 (1), W10 and W16 (2) - measurements 2011.

The colorimetric data point out on the luminance value of frames W10 and W16 the reason - not the origin - of their different behavior (Fig. 4.9).

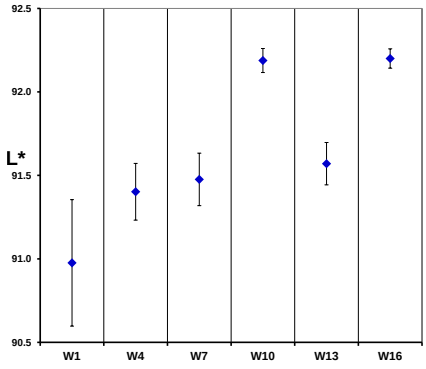

Fig. 4.9: White frames in acrylic binder, untreated areas - W1, W4, W7, W10, W13 and W16. Colorimetric graph of L* parameter- measurements 2011.

In the following, frames W10 and W16 are treated separately from other frames.

4.1.4 Evaluation of artificial aging effects

Titanium white in acrylic binder

Five measurements were performed on part 1 and 4 of frames (Fig. 4.2(a)(b)) W1, W4, W7, W10, W13, W16 (Fig. 4.1(b)).

Fig. 4.10(a) shows a clear separation between the irradiated/non-irradiated parts of W10 and W16 frames, occurring on the first principal component. Therefore it can be argued that the most significant differences are determined from artificial aging. While, the variability between the two frames takes place on the second principal component, confirming their similarity.

A similar behavior is registered for the other white frames even if, in two instances (W7, W13) the second component is needed, for a complete discrimination.

Colorimetric results are shown in Fig. 4.11 highlighting the great contribution of b* ($\Delta b^* \cong 0.3 - 0.5$) in this variation.

Titanium white in oil binder

The irradiation effects are subsequently evaluated for the white layer in a different binder, the linseed oil. Based on PCA analysis performed on reflectance data relative to W6 frame (Fig. 4.12(c)), it is clear that the sharp separation on the first principal component is due to irradiation, although it is not recognizable by visual inspection (Fig. 4.12(a)) and colorimetry (Fig. 4.13).

The PCA on W12 frame data shows that the irradiation effects on such frame are less marked than the W6 frame, since the separation of the two areas is based on the second principal component (Fig. 4.14).

Irradiated blue in oil binder

Unlike from the visible image, the image collected at 490 nm of B6 frame, shows the differences due to artificial irradiation (Fig. 4.15(a), 4.15(b)). Multivariate analysis on the IS spectral data points out more easily these differences (Fig. 4.15(c)).

The same evidence is achieved with PCA on B12 frame data (Fig. 4.16).

By colorimetric data examination, the a* parameter appears responsible of the variations estimated, with $\Delta a^* \cong -1.8 \pm 0.7$ (Fig. 4.17). Therefore, the irradiation effect for the blue layer in oil is manifested as a small toning to green.

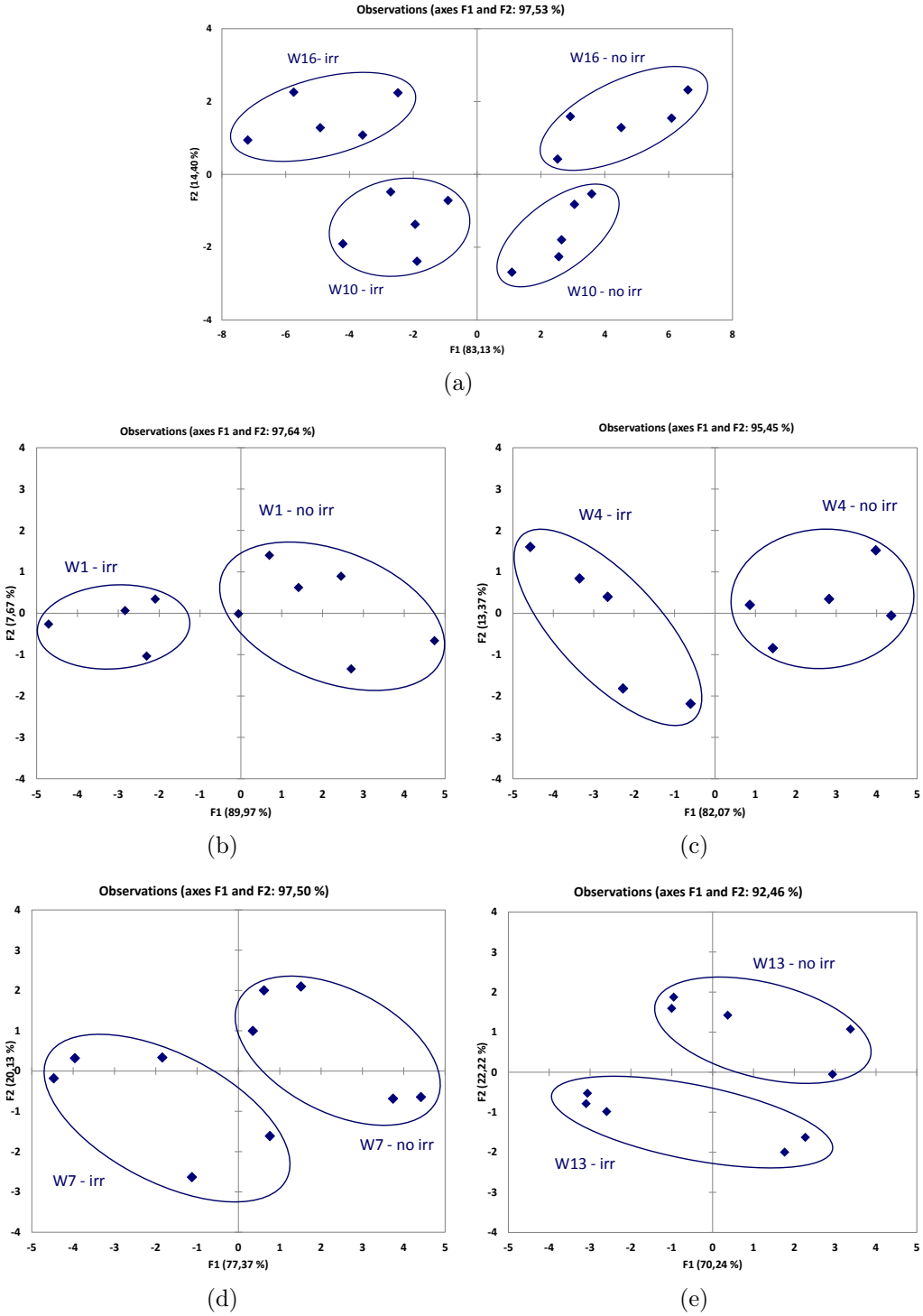

Fig. 4.10: Titanium white in acrylic binder - (a) W10 and W16 frames. PCA results on imaging data of irradiated and non-irradiated parts. W1 (b), W4 (c), W7 (d) and W13 (e) frames. PCA results on imaging data of irradiated and non-irradiated parts.

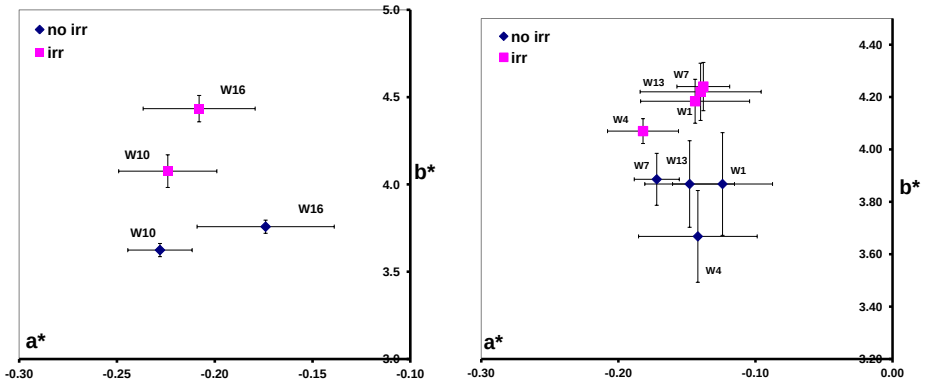

(a) (b)

Fig. 4.11: Titanium white in acrylic binder - W10, W16 (a) and W1, W4, W7, W13 (b) frames. Colorimetric parameters, a* and b*, of irradiated and non-irradiated parts.

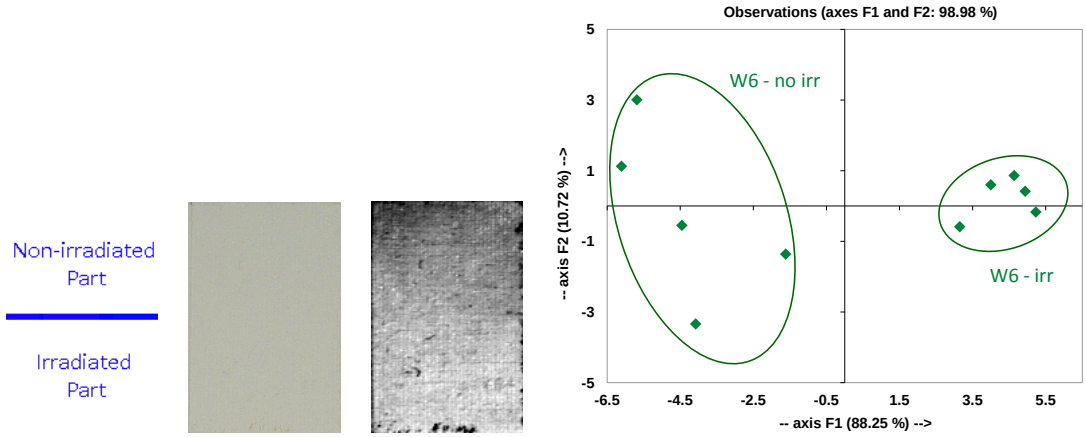

(a) (b) (c)

Fig. 4.12: Titanium white in oil binder - W6 frame. (a) Color and (b) image collected at 490 nm of non-varnished part of W6 frame. (c) PCA results on imaging data of irradiated and non-irradiated parts.

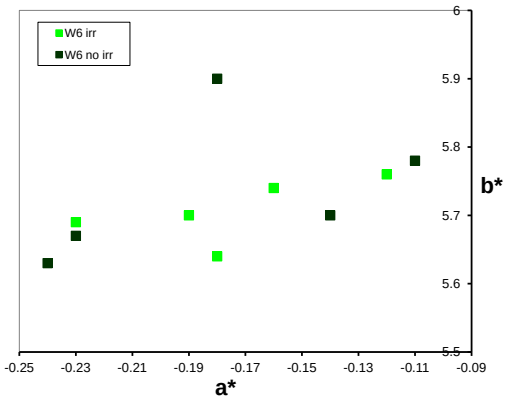

Fig. 4.13: Titanium white in oil binder - W6 frame. b* vs a* plot (b) obtained by contact spectrophotometer on irradiated and non-irradiated parts.

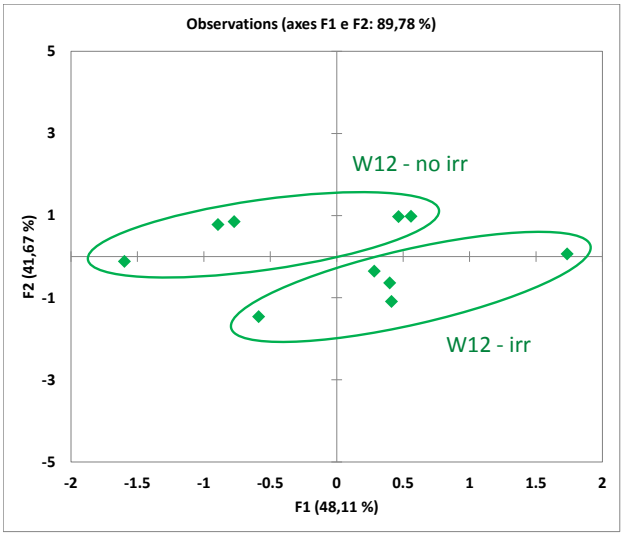

Fig. 4.14: Titanium white in oil binder - W12 frame. PCA results on imaging data of irradiated and non-irradiated parts.

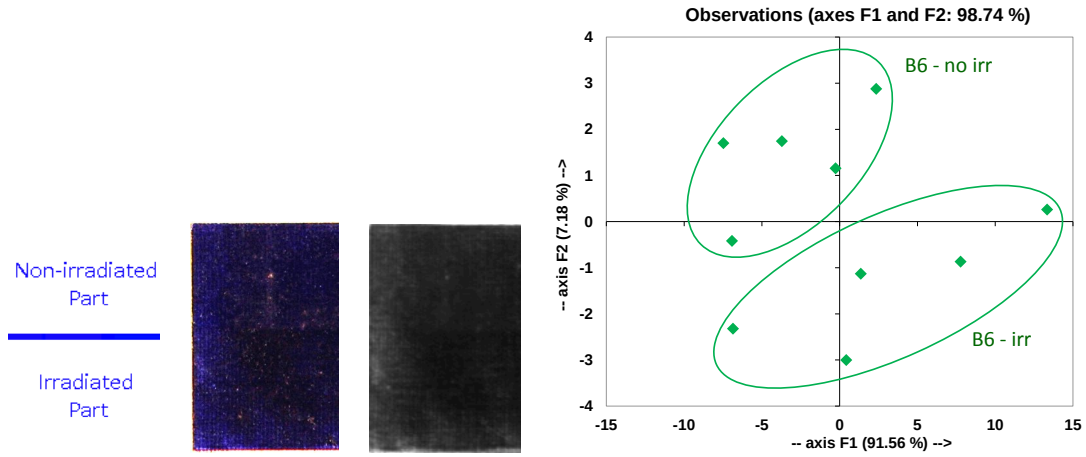

(a) (b) (c)

Fig. 4.15: Artificial Ultramarine Blue in oil binder - B6 frame. (a) Color and (b) image collected at 490 nm of non-varnished part of B6 frame. (c) PCA results on imaging data of irradiated and non-irradiated parts.

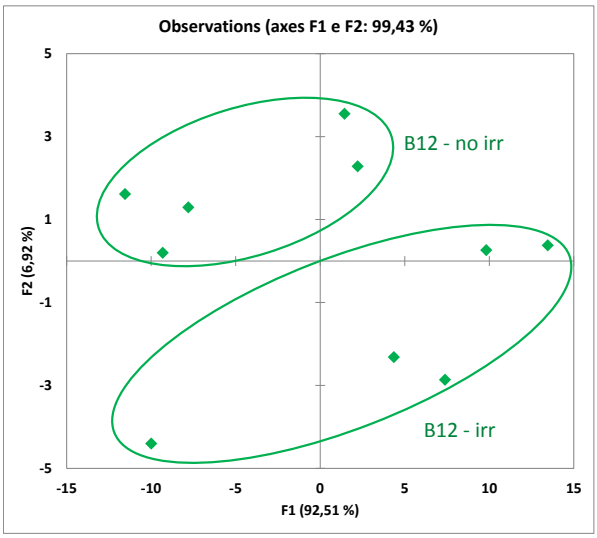

Fig. 4.16: Titanium white in oil binder - B12 frame. PCA results on imaging data of irradiated and non-irradiated parts.

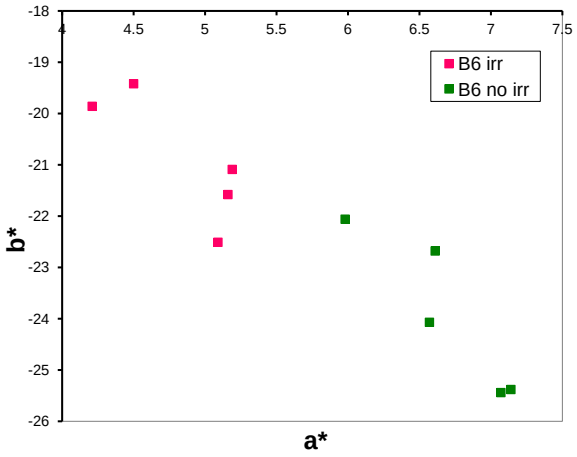

Fig. 4.17: Artificial Ultramarine Blue in oil binder - B6 frame. b* versus a* plot on irradiated and non-irradiated parts.

4.1.5 Natural aging of Titanium white in acrylic binder

Finally, the effects of natural aging are investigated. Titanium white in acrylic binder are taken into account, focusing on W10 e W16 frames, rapresenting a well defined cluster in the previous analysis (Fig. 4.8(b)). The spectrophotometric data of measurements collected in 2003 and 2011, are compared. Irradiated and non-irradiated parts are analyzed separately.

First, for the untreated areas, PCA shows a separation on the first principal component, of the data related to the different years (Fig. 4.18(a)).

Then, the irradiated parts of such frames are considered (Fig. 4.18(b)). The measurements of W10 frame, collected in 2003 and 2011, can be distinguished on the second component. It can be interpreted as the artificial irradiation has caused an early aging of the frames.

Based on the colorimetric analysis, the Lightness L^* seems to be the most sensitive indicator of the variations observed over time (Fig. 4.19). The common trend appears as a reduction in the L^* values. It can be claimed that, regarding the considered frames, after eight years of natural aging they values, similar to those induced in a short time by artificial irradiation have been reached.

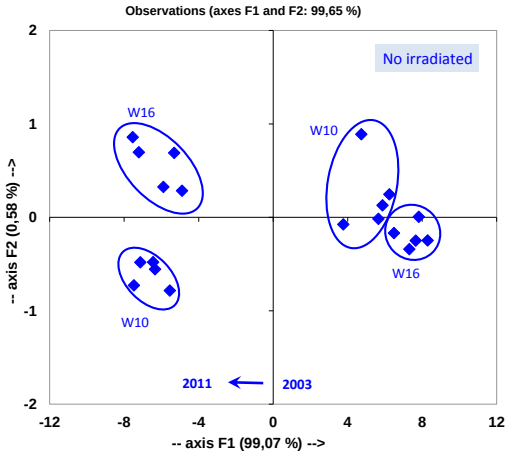

(a)

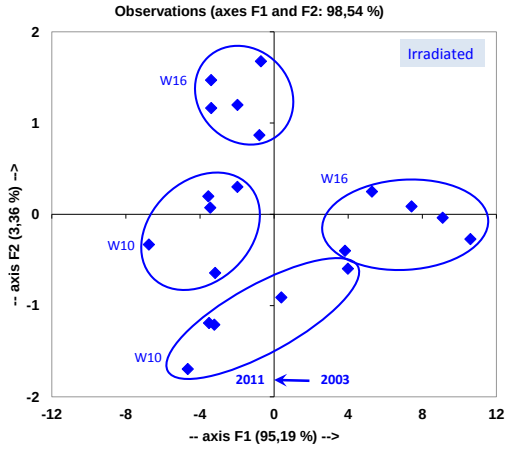

(b)

Fig. 4.18: Titanium white in acrylic binder - W10, W16 frames. (a) PCA results on Spectrophotometer data collected in 2003 and 2011 on irradiated parts and (b) non-irradiated parts.

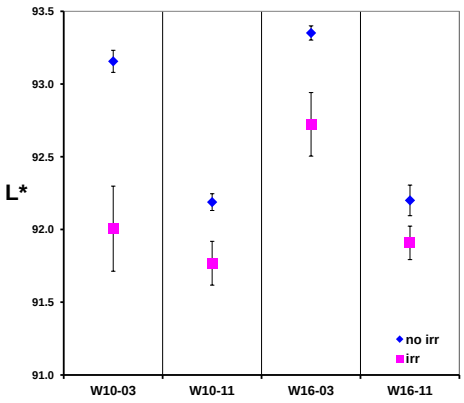

Fig. 4.19: Titanium white in acrylic binder - W10, W16 frames. L* graph for irradiated and non-irradiated parts.

4.2 Authentication of contemporary artworks: the Lithopone case

UV-VIS-NIR reflectance spectroscopy has successfully been used for recognition of pigments used on twentieth-century artworks [27]. As it was demonstrated, this is possible in white pigments, such as lead white, zinc white, titanium white, lithopone and kaolin, by using fiber optic reflectance spectroscopy in the 270-1700 nm spectral range [8]. An application of IS, in which lithopone pigment was distinguished from other white pigments through the different reflectance in a limited spectrum range, is presented here.

Description A test panel was made by oil paint on canvas. Four white pigments layers (Fig. 4.20(a)), such as Lithopone ($ZnS+BaSO_4$), Zinc white (ZnO), Titanium white (TiO_2) and Calcium carbonate ($CaCO_3$) are present.

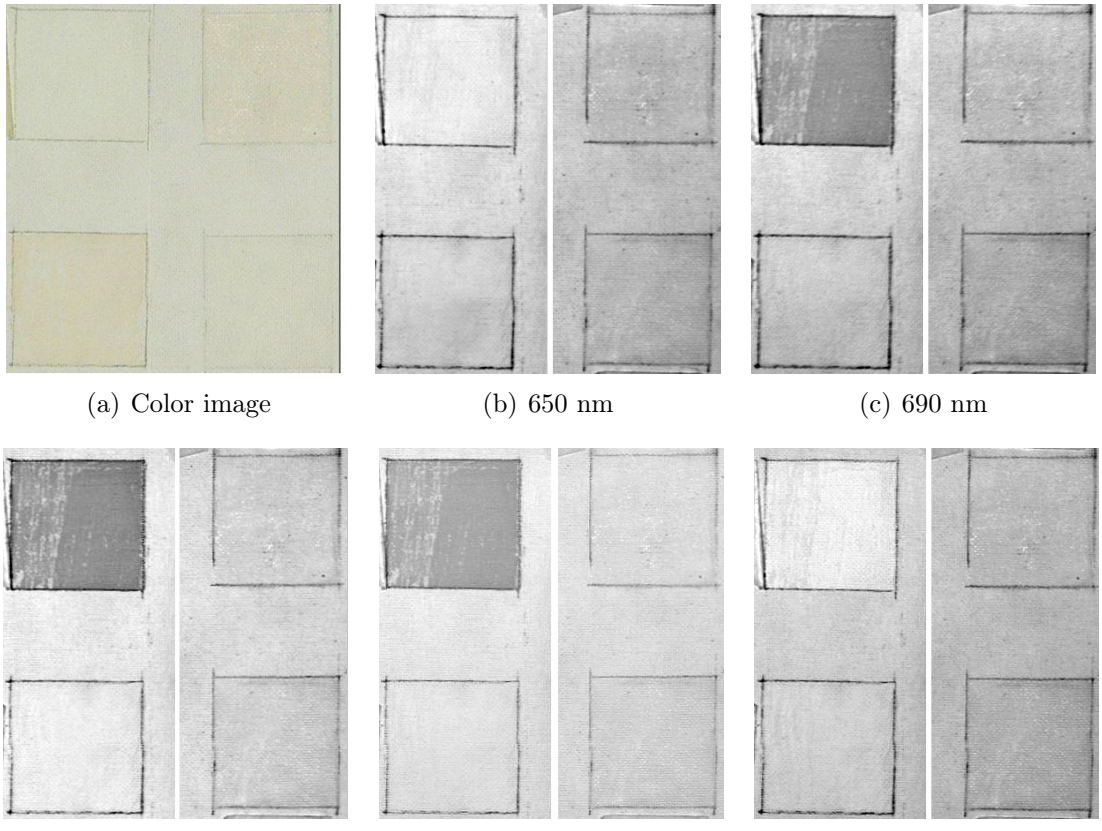

(a) Color image (b) 650 nm (c) 690 nm

(d) 710 nm (e) 730 nm (f) 790 nm

Fig. 4.20: From the upper left and counterclockwise: Lithopone, Zinc white, Titanium white, Calcium carbonate layers on test panel, shown in the visible (a) and at different wavelengths (b-f) acquired by IS. Lithopone layer shows a characteristic behavior at 690 nm, 710 nm and 730 nm.

Lithopone was one of the white pigments widely used in the XX century. It was first prepared in 1847 by precipitating zinc sulfate with barium sulfide, then patented in France in 1850 and finally produced commercially since 1874. Later, it was recognized that a prolonged exposition to sunlight may produce blackening of such pigment due to the formation of finely distributed metallic zinc [35].

A significant enhancement in the production process occurred between 1922 and 1925, when a fraction of cobalt salts was added to the ZnS salt solution, previous purified. The cobalt (0.02-0.5 %) was incorporated into the ZnS lattice during the next stage of calcination, thereby slowing down the deterioration process to which Lithopone was prone [13]. The cobalt can be included in Lithopone molecules as low as 25 ppm [8].

A cobalt (II) ion being in pseudo-tetrahedral sulfur coordination in the zinc sulphide compound, shows an absorption band in the visible region, located around 710 nm [27].

The presence of the cobalt signature may have important applications in artistic field, by allowing a relative dating of the artworks older than the mid-1920s.

The Lithopone's layer in the test panel manifests a blackening in the images collected at 690, 710 and 790 nm, attesting the presence of cobalt as a vicariant element of zinc (Fig. 4.20).

The IS reflectance spectrum for Lithopone, compared with the spectra for the other white pigments, clearly shows an absorption band between 650 and 790 nm, as expected (Fig. 4.21).

The IS is sufficiently sensitive to cobalt, despite of his presence in trace amounts in Lithopone.

The XRF spectrum (Fig. 4.22), obtained with an acquisition of 20 minutes long, shows the characteristic fluorescence peaks of predominant elements, like zinc, barium and sulfur and traces of cobalt (about 1 cps).[1]

Therefore, IS analysis can be more effective than a elemental analysis, as XRF, in order to verify traces of cobalt in Lithopone's pigments.

PCA clearly distinguishes Lithopone from the other white pigments (Fig. 4.24), through the first principal component. By factor loading examination (Fig. 4.23), the discriminant variables for such separation are, of course, the wavelengths of the cobalt dip. Only the titanium white is separated on the second principal component from the other whites.

[1]The XRF analysis was performed by using a Bruker apparatus, Artax 200 model, with Molybdenum anode. The exposure parameters were 25 KV, 1502 μA, 1200 sec. Higher energy values were used, with no evidence of the cobalt signature.

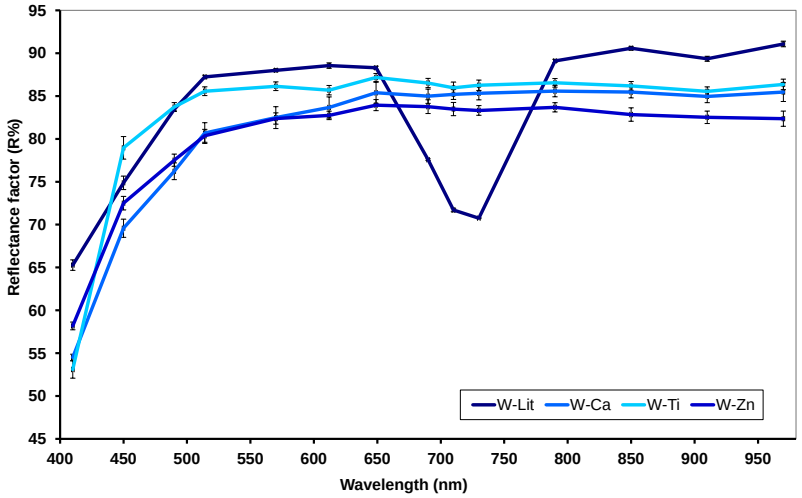

Fig. 4.21: VIS-NIR reflectance spectrum of the white pigments.

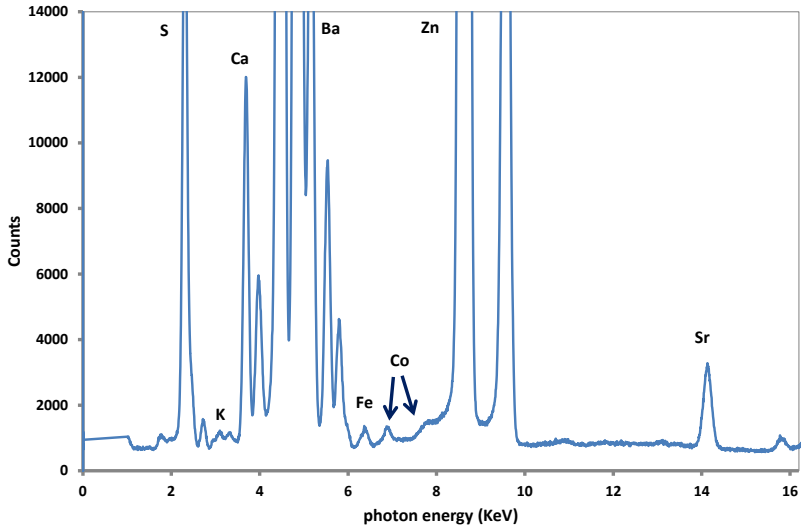

Fig. 4.22: XRF spectrum of Lithopone.

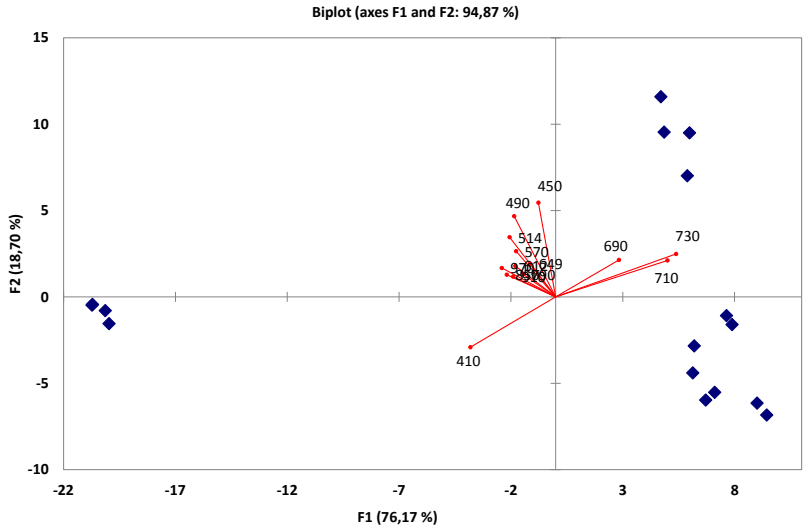

Fig. 4.23: Biplot graph obtained by PCA on four whites layers. The data separation on the first PC is due to 690, 710 and 730 nm wavelengths.

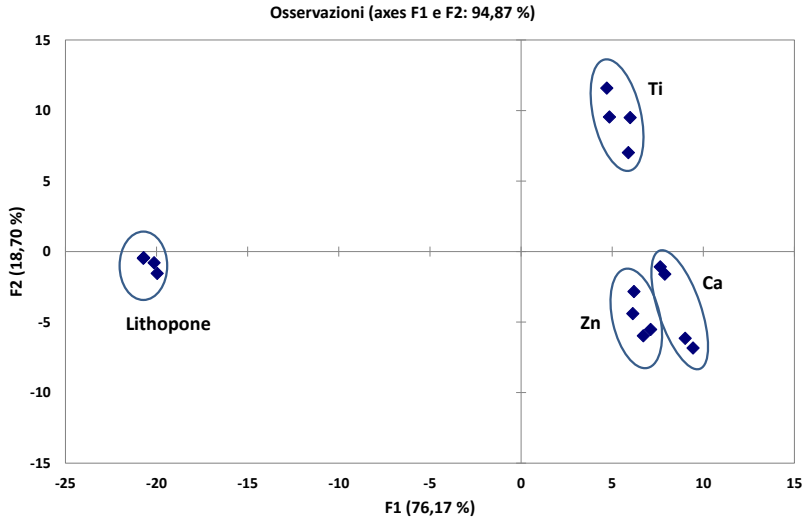

Fig. 4.24: PCA results of four whites layers.

4.2.1 Lithopone panel: monitoring the state of conservation

The time evolution of the Lithopone test panel is evaluated, by comparing such measurements with those carried out two years ago. In Fig. 4.25 the results are shown. An underway aging of this layer is evident by PCA graph, with a separation of the two clusters on the first principal component (Fig. 4.25(a)). While, by observing a* and b* colorimetric parameters in Fig. 4.25(b), the ageing trend appears yellowing, with a mean variation of +2 in b* values.

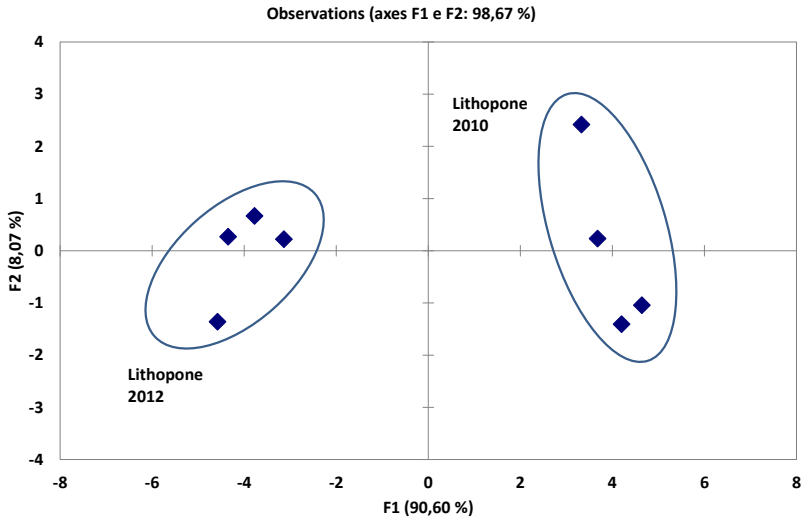

(a)

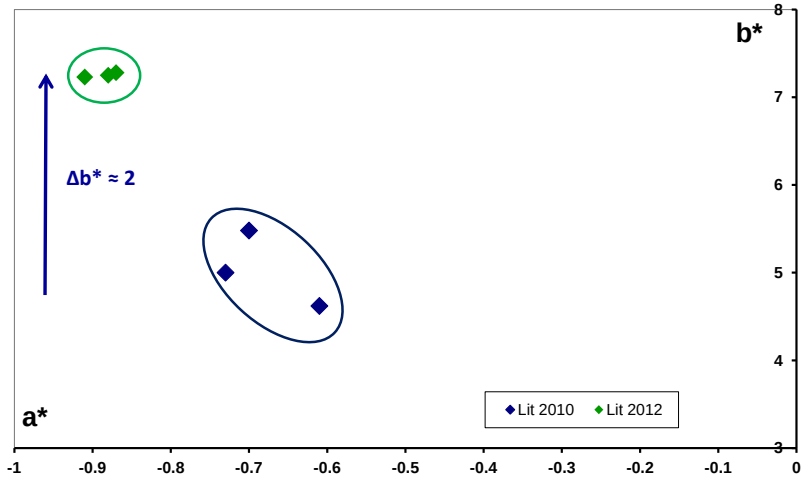

(b)

Fig. 4.25: Results of measurements after an interval of two years on Lithopone by PCA (a) and by colorimetric analysis (b).

4.3 *Contrast of forms*, Peggy Guggenheim Collection, Venice

The painting is part of the Peggy Guggenheim Collection (PGC) in Venice, since it was bought by Peggy Guggenheim in the late 1960s. It supposedly belongs to the series of *Contrast of forms*, painted by Fernand Léger from the late summer of 1913 up to August 1914 (Fig. 4.26).

Fig. 4.26: *Contrast of forms*, oil on canvas, 92 x 73 cm, P. Guggenheim Collection, Venice

The first documentation concerning the work dates back to 1950s.

Because of some perplexity about his authenticity, raised by the art critic Douglas Cooper at the end of Seventies, a scientific survey was carried out for attesting

the presence of some anachronistic element with the supposed date of the work. Infrared reflectography, X-ray radiography, spectrophotometry with integrating sphere and SEM-EDS analysis were performed in recent years on the painting. Three large portions of the painting were inspected by IS (Fig. 4.27).

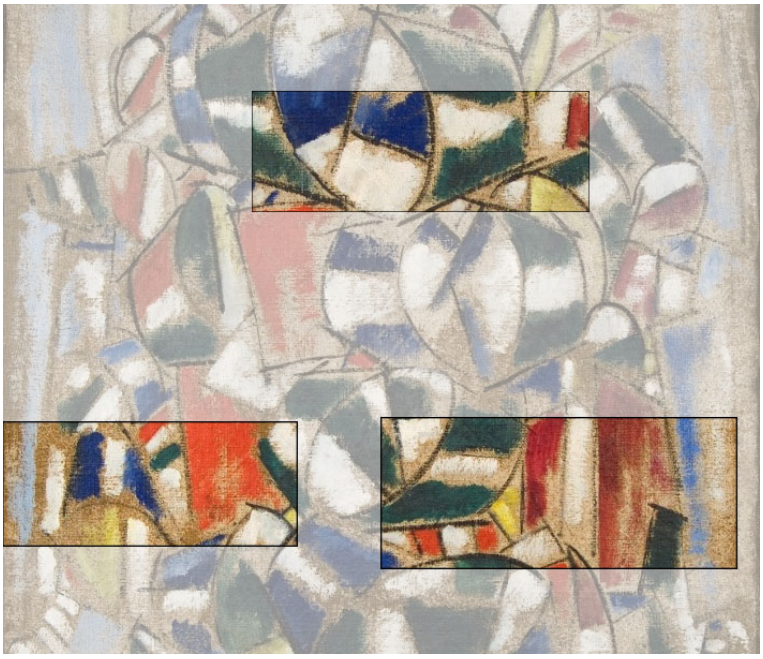

Fig. 4.27: *Contrast of forms*, oil on canvas, 92 x 73 cm, P. Guggenheim Collection, Venice. Selected areas for IS acquisition.

White colors

The examination of white colors by SEM-EDS revealed the use of Lithopone, due to the presence of Sulfur, Barium and Zinc (Fig. 4.29(a)).

Through the images acquired by IS, the white areas appear darker at 710 nm than at 690 nm and 730 nm images (Fig. 4.28).While, the spectral results obtained by IS images elaborations clearly show the cobalt absorbtion band, from 650 nm to 790 nm (Fig. 4.29(b)).

Even if the Lithopone layer was blemished by the dirty brush, a faint absorption in this spectral range it is still visible, like in the case of W1 reflectance spectrum.

By identifying the cobalt in the Lithopone brushstrokes, the authenticity of the work can be refused. Accordingly, the Venetian painting was executed after the period in which Léger painted the *Contrast of forms* series.

A final word on the authentication was given by radiocarbon dating of the canvas, resulting not preceding to 1955.

(a) color image of Lithopone layers

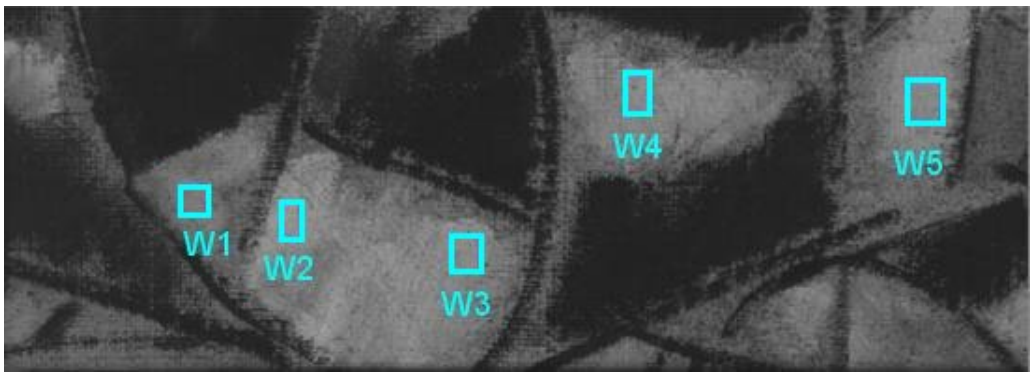

(b) 650 nm

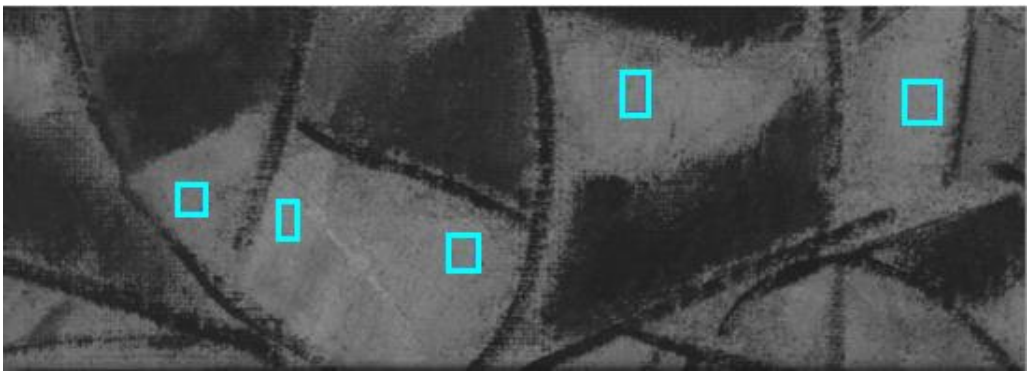

(c) 710 nm

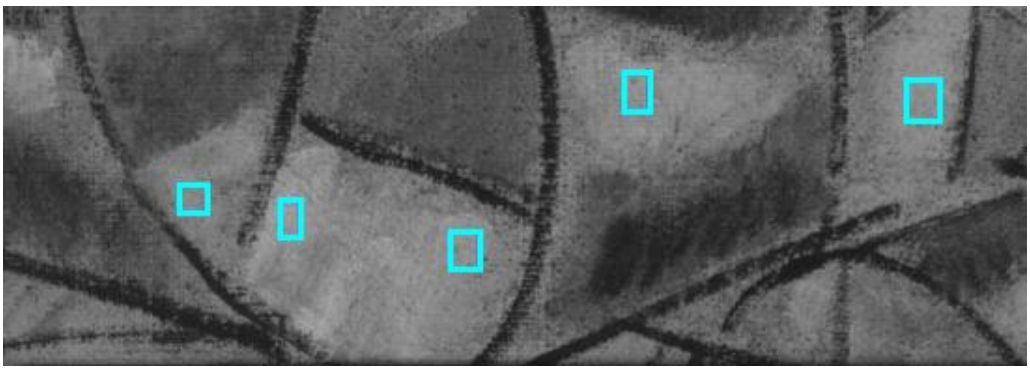

(d) 790 nm

Fig. 4.28: *Contrast of forms*, PGC, Venice. Images acquired at different wavelengths of one area investigated by MIS. Lithopone layers reflect differently the light at the three wavelengths. At 710 nm it appears darker than 650 nm and 790 nm. In light blue the Lithopone zones where reflectance spectral information were achieved.

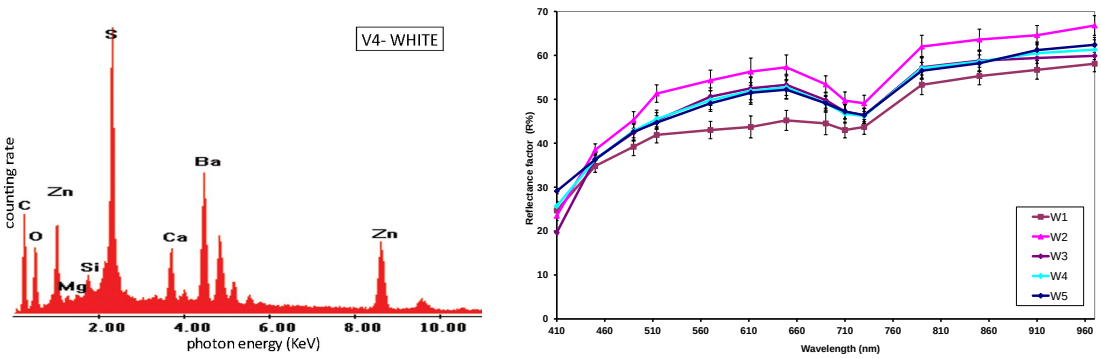

(a) (b)

Fig. 4.29: *Contrast of forms*, PGC, Venice. EDS and IS spectra of the Lithopone.

Blue colors

For the blue pigments the presence of silicon, aluminum and sulfur, in the EDS spectra (Fig. 4.29(a)), strongly suggests the use of Ultramarine Blue ($Na_{8\text{-}10}Al_6Si_6O_{29}S_{2\text{-}4}$). The reflectance spectrum is useful to confirm the use of a white pigment to create the pale blue tints, increasing the reflectance values (Fig. 4.29(b)). By EDS analysis, it seems to be Lithopone white, due to the presence of Sulfur, Barium and Zinc (Fig. 4.29(a)).

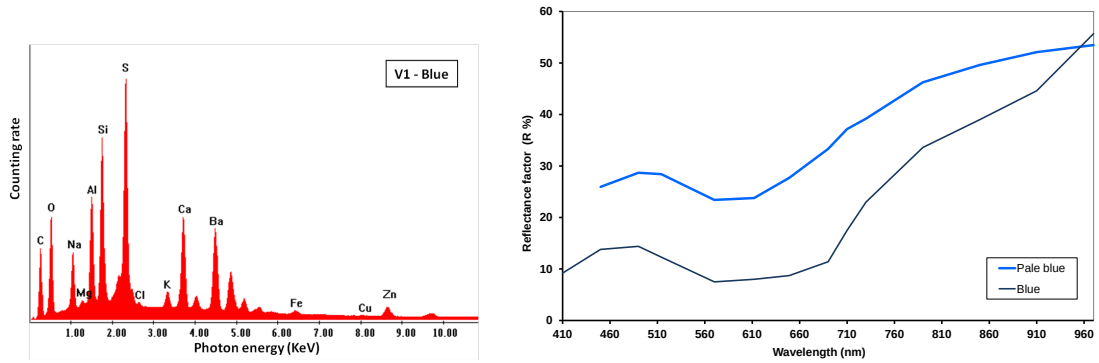

(a) (b)

Fig. 4.30: *Contrast of forms*, PGC, Venice. EDS and IS spectra of the blue pigments.

Green colors

For the green color, the EDS spectrum shows the chromium as prevailing chemical element, solely responsible for the green coloration (Fig. 4.31(a)). For this

reason, the Cinnabar Green ($Fe_4[Fe(CN)_6]_3 + PbCrO_4$)can be excluded.

The IS reflectance spectrum was able to discriminate between the last two probable pigments. The reflectance maximum around 490 nm and the increase in reflectance at about 710 nm (Fig. 4.31(b)), steady in the NIR range, suggest the presence of Viridian ($Cr_2O_3 \cdot 2\,H_2O$), while the Chrome Green (Cr_2O_3) would have two peaks at 410 and 535 nm [10].

Where the green pigment was mixed with a black one, the final results is an overall dramatic downward trend of reflectance values. The use of black pigment is highlighted in the middle part of Fig. 4.28, since the green layers become transparent in the infrared range while the black brushstrokes remain strongly opaque.

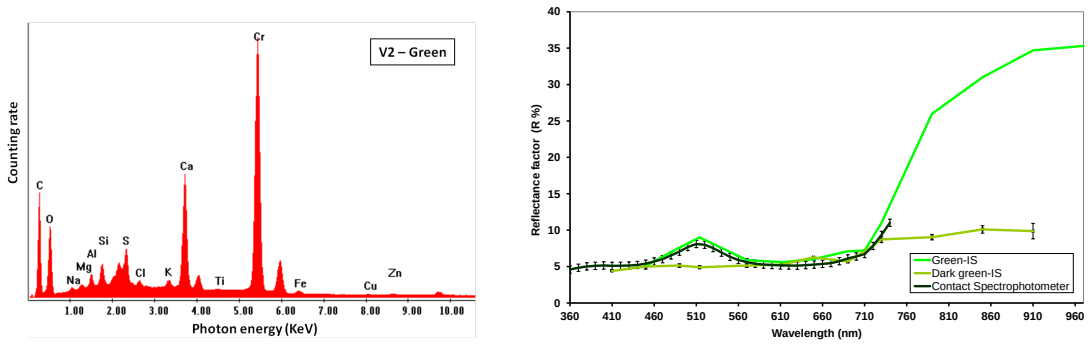

(a) (b)

Fig. 4.31: *Contrast of forms*, PGC, Venice. EDS and IS spectra of the green pigments.

4.4 *Landscape* by Guglielmo Ciardi

This painting by Guglielmo Ciardi (1842-1917) represents a country landscape, which was one of preferred subjects of the Venetian artist (Fig. 4.32). It is an oil paint on wooden panel.

The images acquired by IS show an overall low reflectance of pigments until 610 nm (Fig. 4.33). Higher reflectance values are observed at 690 nm, mainly for the blue layers used for the mountains. While in the near infrared range pictorial materials are overall highly transparent. Only the pigment used for the windows and the dark green used for the trees remain opaque.

Fig. 4.32: Guglielmo Ciardi, *Landscape*, oil on wooden panel, end of XIX cent., 20x15 cm, private collection.

The reflectance spectrum obtained by IS and by contact measurements on blue layers, compared with blue spectra presents on reference database, seems to be a cobalt based pigment with a reflectance maximum at about 510 nm and higher reflectance values from 700 nm (Fig. 4.34). In the near infrared range from 1000 nm, these pigments show a sharp reflectance fall (Fig. 4.34(b)) to become deep dark at higher wavelengths, from 1300 nm [16].

The wide band infrared reflectography, fitted with an InGaAs detector (1000-2500 nm), shows clearly this characteristic behavior with a darkening of mountain brushstrokes (Fig. 4.35).

(a) 610 nm

(b) 690 nm

(c) 850 nm

Fig. 4.33: Guglielmo Ciardi, *Landscape*. Images acquired at different wavelengths, 610 nm, 690 nm, 850 nm, of one investigated area by MIS.

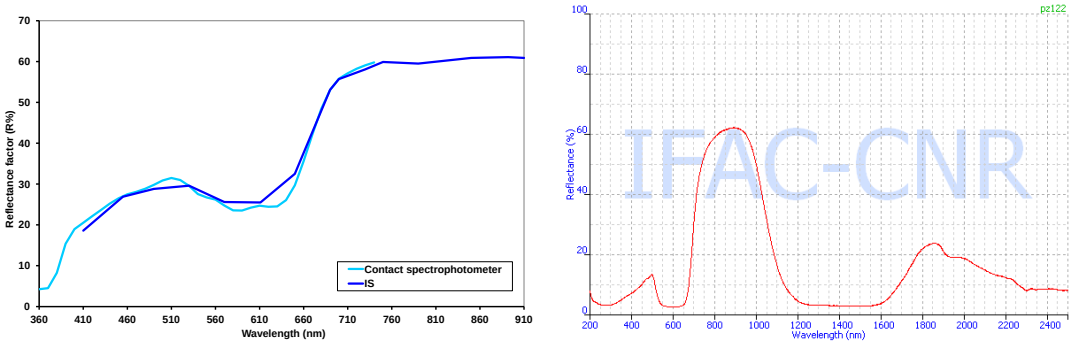

(a) (b)

Fig. 4.34: Guglielmo Ciardi, *Landscape*. (a) IS spectrum, compared with contact spectrophotometer spectrum, of blue pigment used for the mountains. (b) Reference spectrum of Cobalt blue [26].

Fig. 4.35: Guglielmo Ciardi, *Landscape*. Wide band infrared reflectography with InGaAs detector.

4.5 *At the Cycle-Race Track* by Jean Metzinger

To the painting *At the Cycle-Race Track* by Jean Metzinger (1883-1956) was devoted to an exhibition on the occasion of its centenary. It portrays the winner of the race Paris-Roubaix 1912, Charles Crupelandt, just a moment before of crossing the line. It is a cubist work, where the artist represents movement.

Description

The support of the painting is a linen canvas. The pictorial layer is characterized by particles of different granulometry associated with the oil paint and applied by brush.

An in-depth study was carried out in order to investigate the pictorial technique and the materials by using several noninvasive image diagnostics [29].

The results concerning the reflectance spectral behavior in the VIS-NIR range of the materials constituent the work is presented here. XRF results[2] will be taken into account for pigment identification purposes [7]. Three are the areas investigated by IS, shown in Fig. 4.34.

Blue colors

The XRF analysis on blue layer depicting a flag on the top of the painting Fig. 4.38(a), pointed out the absence of elements characterizing the most common blue pigments, like cobalt, copper (Fig. 4.38(b)). This could be a Prussina Blue ($Fe_4[Fe(CN)_6]_3 \cdot nH_2O$), an organic pigment as Indigo ($C_{16}H_{10}O_2N_2$) or a pigment with low atomic number elements as Ultramarine Blue ($Na_{8\text{-}10}Al_6Si_6O_{29}S_{2\text{-}4}$), not-detectable.

Compared with XRF analysis, the IS inspection performed on blue layers on the face of the rider showed in Fig. 4.39(a), allows to exclude Prussian Blue and Indigo, since the spectrum of the first pigment should rise over the 900 nm, while the Indigo spectrum should appear flat in the visible range. By examining the reflectance spectrum in Fig. 4.39(b) it can be inferred that the peak around 450 nm is due to Ultramarine blue. The reference reflectance spectrum of Artificial blue ultramarine confirms such assumption (Fig. 4.40(b)).

By examining the pale blue layers, from XRF analysis can be excluded Azurite, Prussian Blue and cobalt-based blue. However, chromium and cadmium have been revealed here. Although it is not possible to reach a unique conclusion, the reflectance spectrum suggests the use of two different blue pigments. The last one differs from that of the Ultramarine blue for a peak well over 490 nm and a marked increase of reflectance over 650 nm.

[2]XRF analysis was carried out with the collaboration of Paola Artoni, Non-invasive analysis laboratory for ancient and modern works of art, University of Verona.

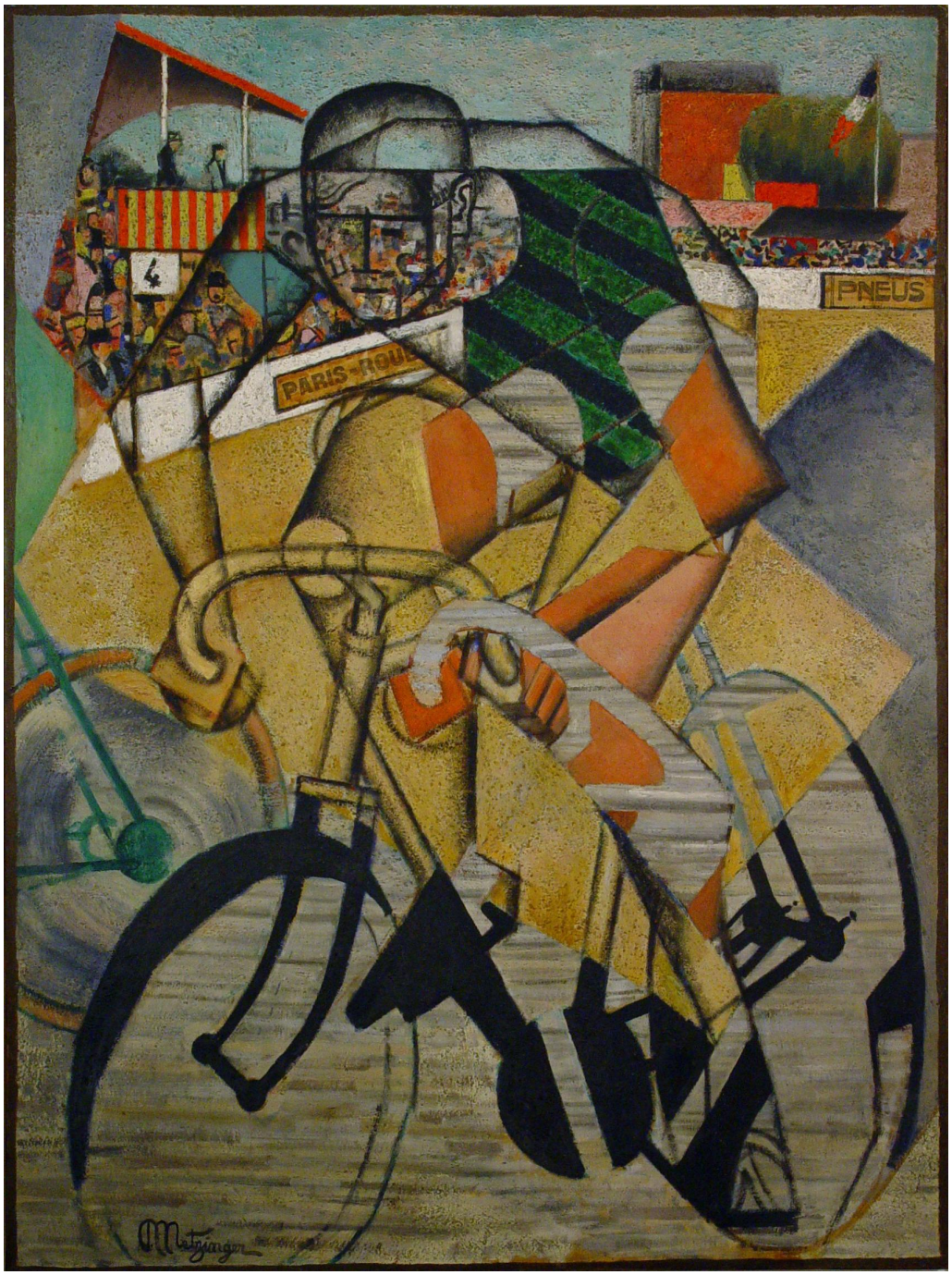

Fig. 4.36: Jean Metzinger, *At the Cycle-Race Track*, 1912, Oil and collage on canvas, 130.4 x 97.1 cm, Peggy Guggenheim Collection, Venice.

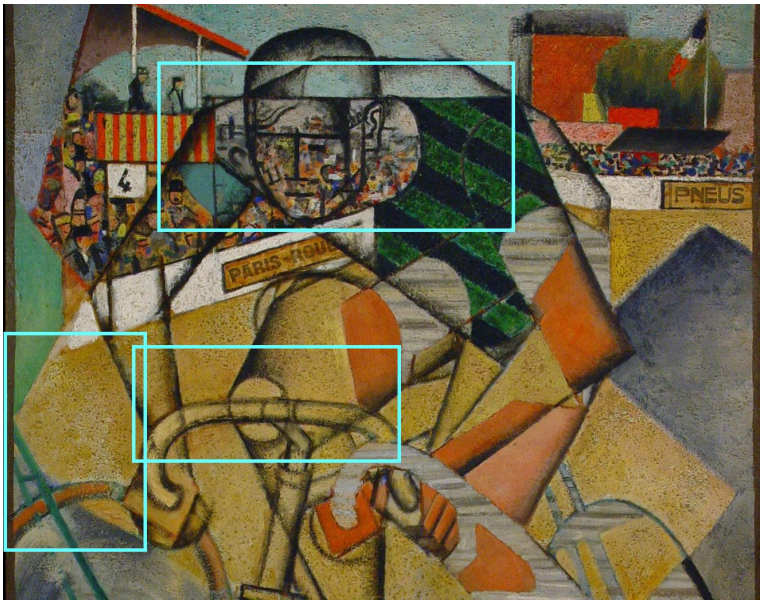

Fig. 4.37: Jean Metzinger, *At the Cycle-Race Track*, PGC. Selected areas for IS acquisitions.

Green colors

The work has two different tones of green, one lighter (V1, V2, V5, V7) and one darker green (V3, V4), as show by Fig. 4.42(a).

The dark green is used for the green strips of T-shirt of cyclist. The XRF spectrum suggests the use of arsenic and copper compound, most likely Veronese Green $Cu(CH_3COOH)_2{\cdot}3\,Cu(AsO_2)_2$ (Fig. 4.42(b)).

The spectral trend seems to validate such evidence. The reflectance spectra of the three measurement ROIs (Fig. 4.43) are in agreement with the reference spectrum of Veronese green (Fig. 4.44), revealing a steady absorption over 650 nm.

The light green in XRF analysis has a higher content of chromium compared to the dark green, no copper and a significant presence of cadmium (Fig. 4.45).

This makes it possible to think to a chromium-based green, like Chromium oxide (Cr_2O_3) or Viridian ($Cr_2O_3{\cdot}2\,H_2O$). The VIS-NIR spectra does not discriminate between these two pigments, but it may be argued that the greens of the three areas differ only in the amount of white pigment in mixture, since they have a similar trend in the investigated spectral range (Fig. 4.47).

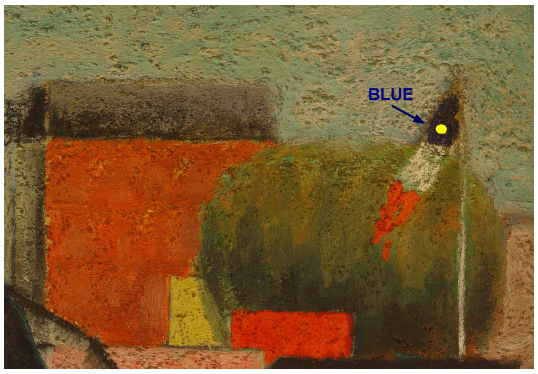

(a)

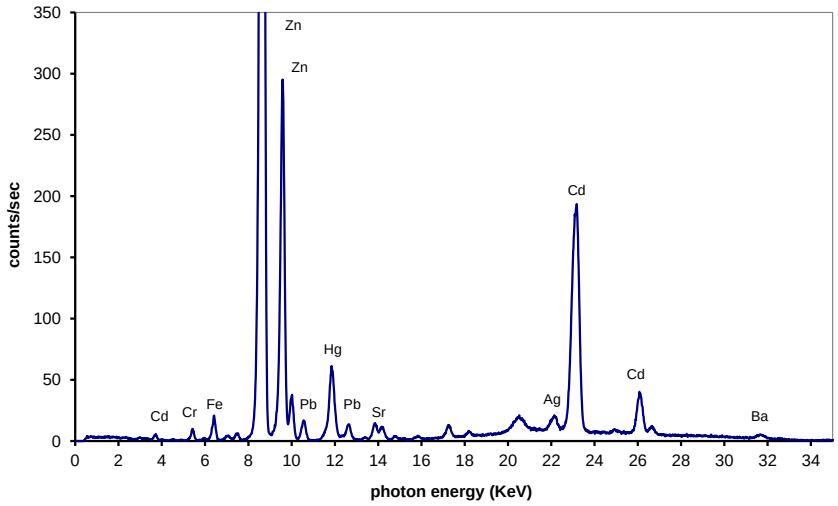

(b)

Fig. 4.38: J. Metzinger, *At the Cycle-Race Track*, PGC. Blue layer (a) of which XRF spectrum is obtained (b).

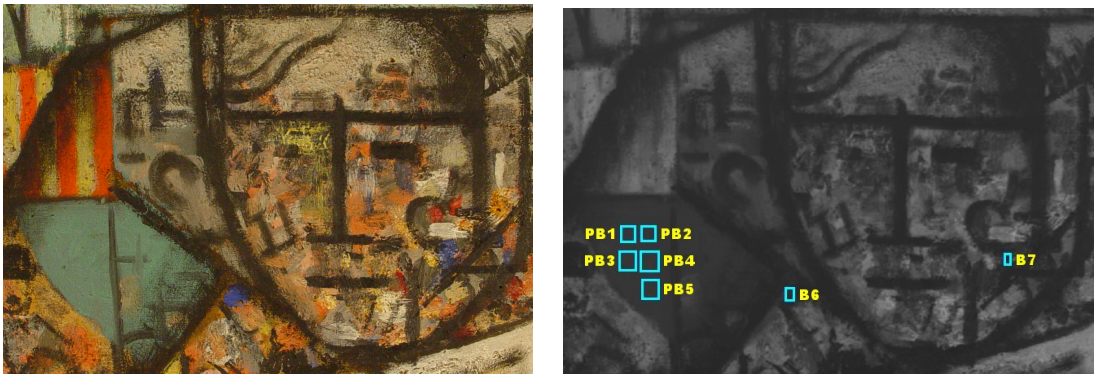

(a) (b)

Fig. 4.39: J. Metzinger, *At the Cycle-Race Track*, PGC. (a) Detail in diffuse light; (b) Detail of image acquired by IS at 650 nm. Measurements ROIs on pale blue and blue areas are shown.

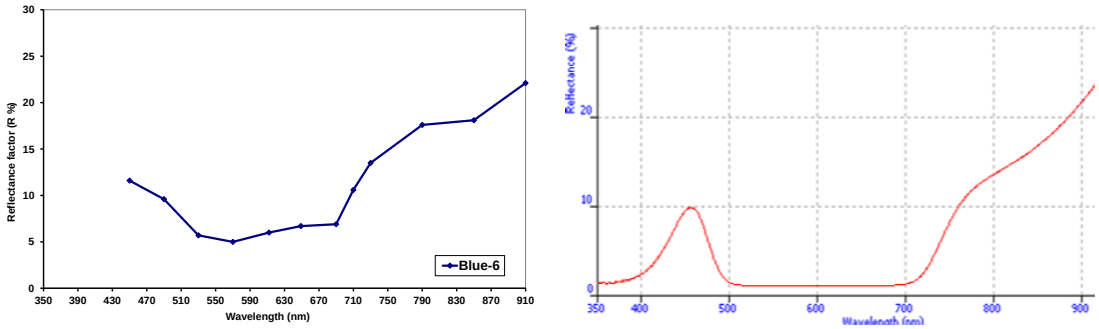

(a) (b)

Fig. 4.40: J. Metzinger, *At the Cycle-Race Track*, PGC. (a) VIS-NIR reflectance spectrum of blue layer; (b) Reference reflectance spectrum of artificial blue ultramarine. From: http://fors.ifac.cnr.it/

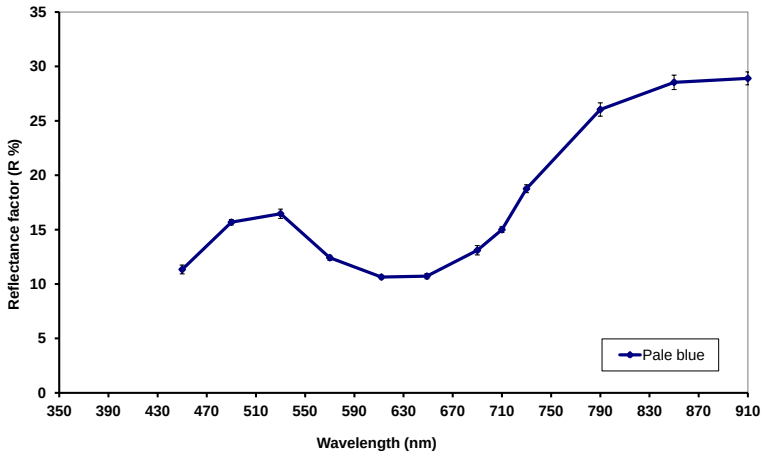

Fig. 4.41: Jean Metzinger, *At the Cycle-Race Track*, PGC. Mean VIS-NIR reflectance spectrum of pale blue.

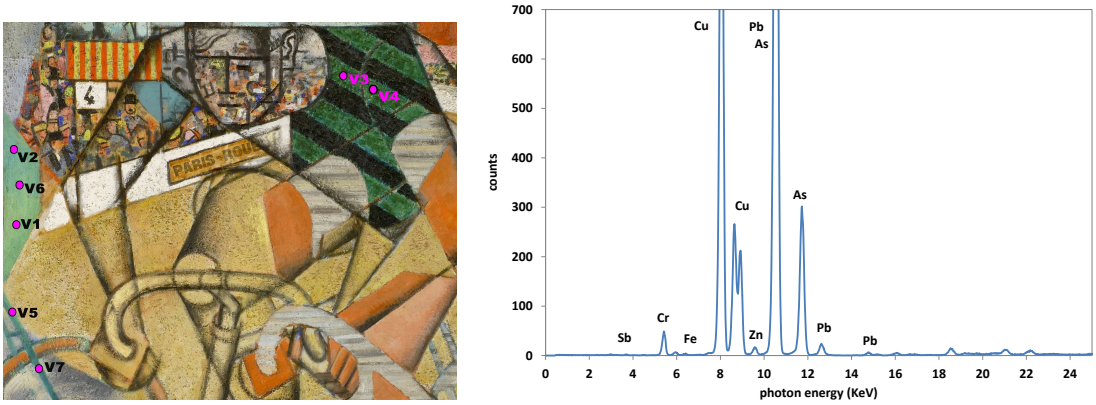

(a) (b)

Fig. 4.42: J. Metzinger, *At the Cycle-Race Track*, PGC. (a) XRF sampling points on dark green layers (b) XRF spectrum of the point V4 on dark green.

Fig. 4.43: J. Metzinger, *At the Cycle-Race Track*, PGC. Image acquired by IS at 530 nm, with measurements ROI on dark green areas G1, G2, G3.

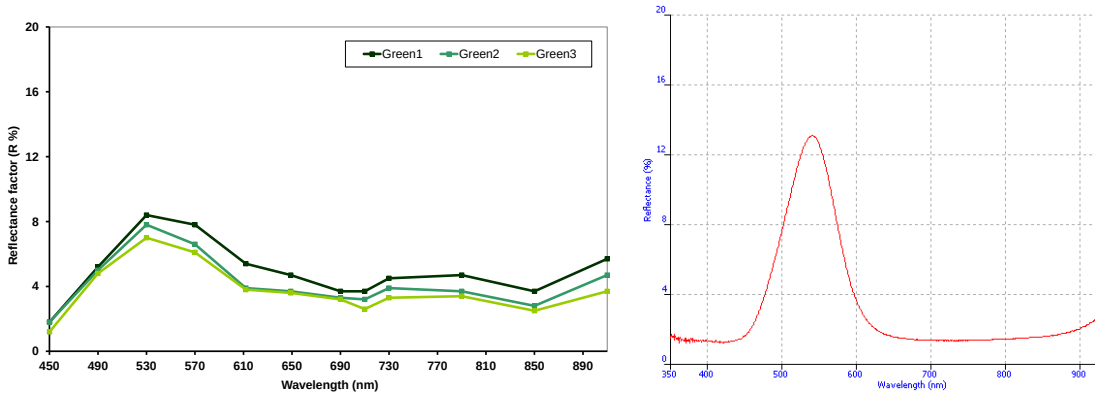

(a) (b)

Fig. 4.44: J. Metzinger, *At the Cycle-Race Track*, PGC. (a) VIS-NIR reflectance spectrum of greens layer; (b) Reference reflectance spectrum of Veronese green. From: http://fors.ifac.cnr.it/

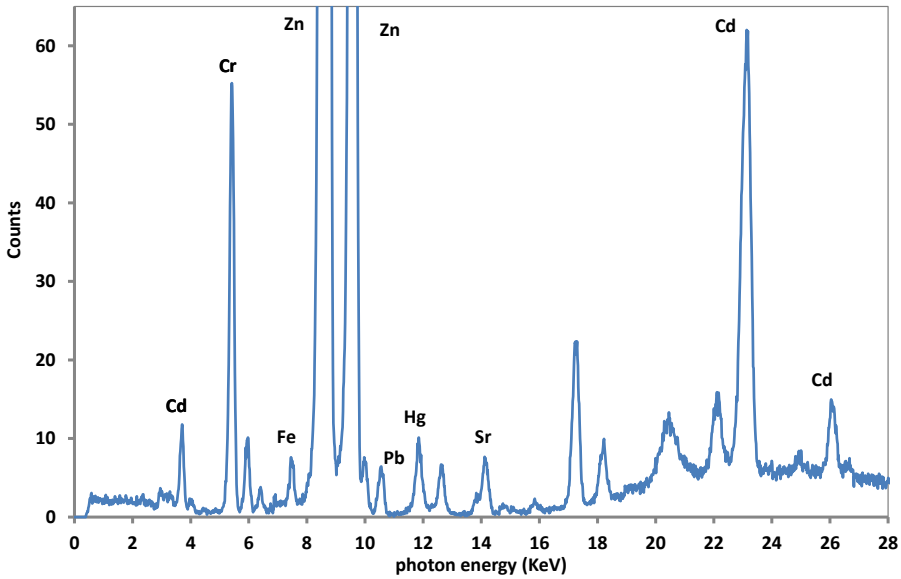

Fig. 4.45: Jean Metzinger, *At the Cycle-Race Track*, PGC. XRF spectrum of the point V1 on light green.

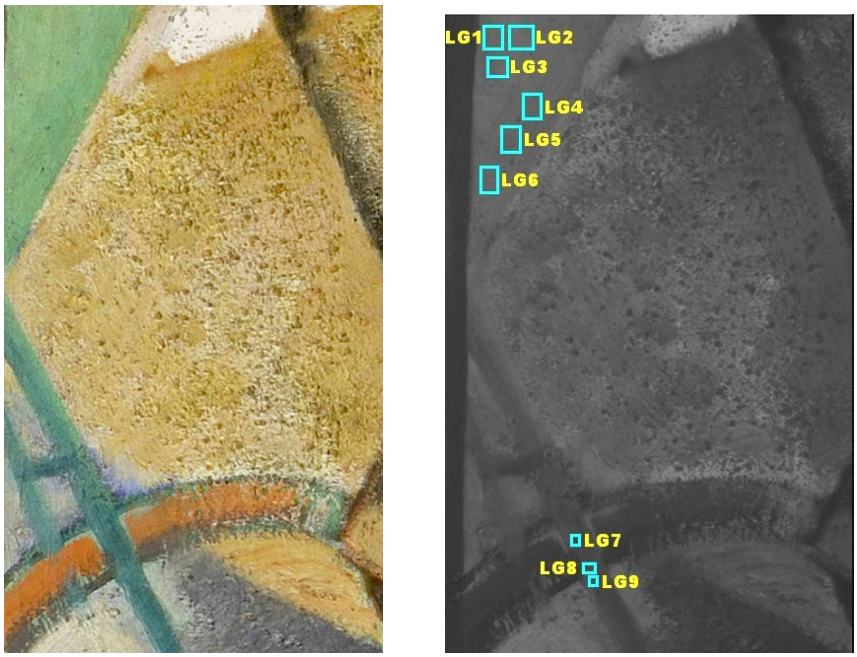

(a) (b)

Fig. 4.46: J. Metzinger, *At the Cycle-Race Track*, PGC. (a) Detail in diffuse light (b) Image acquired by IS at 530 nm, with measurements ROI on light green areas, LG1-LG9.

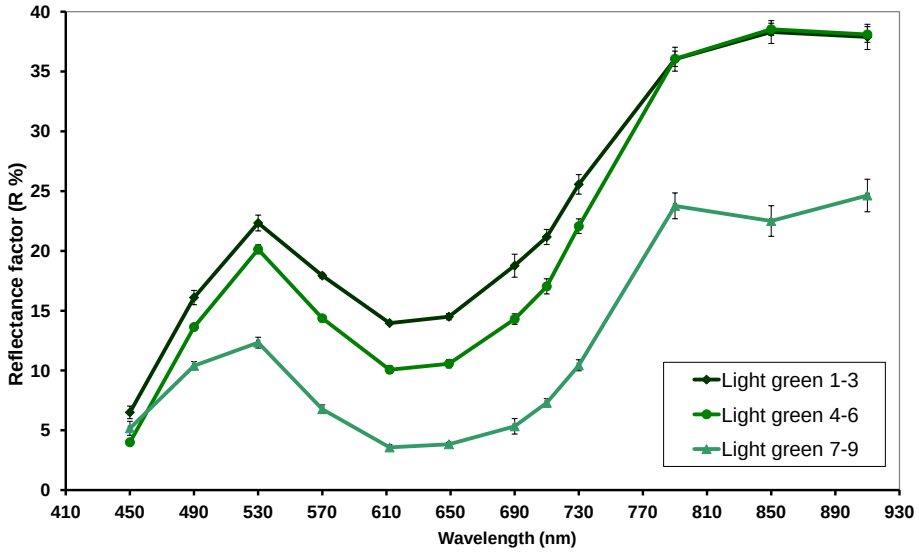

Fig. 4.47: Jean Metzinger, *At the Cycle-Race Track*, PGC. Mean VIS-NIR reflectance spectra of light green.

Conclusions

In this work we focused on Image Spectroscopy (IS) to improve the system in investigating pictorial materials. The method has been applied on some artworks with encouraging results.

First, an effort in improving the multispectral device was made, attempting a full spectrum coverage by selectable bandwidth filters. This method proved to be ineffective in identifying colors and their alterations, so a sparse spectral sampling has been adopted.

Then, the use of Principal Component Analysis on IS spectra has been applied to modern painting materials, as Titanium White, Artificial Ultramarine Blue in acrylic and oil binders in a test panel. $IS + PCA$ has proven to be an effective method for the early identification of chromatic alterations, although of faint amounts. Moreover, colorimetric data have provided useful and complementary information, recognizing the alterations trends.

Unexpectedly, IS has also demonstrated a discriminant power for some materials. The most striking case was the identification of white Lithopone for an absorption band in the visible range, due to the presence of cobalt as vicariant element of Zinc. The knowledge of changes in the chemical composition of this pigment in a specific time period has allowed the recognition of a fake in contemporary artwork. Therefore, significant indications can be obtained by studying contemporary materials, using the knowledge gained outside the merely artistic field.

Appendix A

Geometries of irradiation and observation for the Image Spectroscopy acquisitions

In order to enhance the comparability of results of Image Spectroscopy we report here the calculations of the solid angles of irradiation and observation according the CIE recommendations.

Subsequently, the criteria for which the geometries used in IS can be considered equivalent to those of other devices will be clarified.

Despite to the variability of painting dimensions, IS acquisitions were relatively uniform in size: 20x30 cm^2 is the mean field of view for all paintings examined in this work. Thus, the distance between lamp and painting was also stable and approximately 2.30 m. The same distance, 2.30 m, was kept between painting and camera.

The lamps were arranged at 45 °, ±2 ° with respect to the painting.

Two halogen lamps with large reflector, 31 cm in diameter, were used. The camera lens of the IS device was 5 cm in diameter.

The relation [25]

$$\Omega = 2\pi\Big[1 - \cos\Big(\frac{\alpha}{2}\Big)\Big]$$

and its reciprocal,

$$\alpha = 2\arccos\Big[1 - \Big(\frac{\Omega}{2\pi}\Big)\Big]$$

are used to convert solid angle Ω in plane angle α and conversely.

The following table gives the results for the aperture angles, to be compared

with the CIE recommended limits (Table 2.1): 7.7 ° and 1.25 ° against 8 °.

Colonna1	device radius	device area	distance	solid angle	plane angle
	m	m^2	m	sr	°
irradiation angle	0.155	7.55E-02	2.3	1.43E-02	**7.72**
observation angle	0.025	1.96E-03	2.3	3.71E-04	**1.25**

Fig. A.1: Angles of irradiation and observation for the IS acquisitions.

Painting surfaces are usually good light diffusers, with exception for varnish. A particular care was always kept in avoiding specular diffusion from the imaged portion. By this way, the probability of polarization of the reflected light is indeed very low, thus removing the greatest reason of non-reciprocity of light rays. According to what has been as far shown, measurements by IS give the *spectral reflectance factor in* 2x45 °/ 0 ° geometry.

Bibliography

[1] Albertin F., Boselli L., Gambaccini M., Peccenini E., Pellicori V., Petrucci F., Tisato F., 2011. *Wide band IR reflectography.* In: The 11th International Workshop on Advanced Infrared Technology and Applications AITA, L'Aquila, "Giorgio Ronchi " Foundation, Firenze, p. 28.

[2] Albertin F., Boselli L., Peccenini E., Pellicori V., Petrucci F., Tisato F., 2011. *Spettroscopia in riflettanza per il monitoraggio di materiali pittorici contemporanei.* In: SIOF, Proceedings of VII National Color Conference, Rome, Maggioli Ed., Rimini, Vol. VII/A, pp. 576 - 583.

[3] Albertin F., Boselli L., Peccenini E., Pellicori V., Petrucci F., Tisato F., 2012. *Image spectroscopy for conservation and diagnostics of contemporary painting materials.* In: AIAr, Proceedings of the Meeting "Science for Contemporary art", Ferrara, Patron Ed., Bologna, pp. 93 - 102.

[4] Albertin F., Boselli L., Peccenini E., Pellicori V., Petrucci F., Tisato F., 2012. *Image diagnostics on some paintings of the Remo Brindisi collection.* In: AIAr, Proceedings of the Meeting "Science for Contemporary art", Ferrara, Patron Ed., Bologna, pp. 19 - 27.

[5] Albertin F., Boselli L., Labate M., Peccenini E., Pellicori V., Petrucci F., Tisato F., 2012. *Caratterizzazione dei materiali di un dipinto mediante radiografia differenziale al K-edge e XRF.* In: AIAr, Proceedings of VII Archaeometry National Meeting, Modena, Patron Ed., Bologna, pp. 874 - 885.

[6] Aldrovandi A., Picollo M., 2007. *Metodi di documentazione e indagini non invasive sui dipinti.* Il Prato Ed., Padova, Italy.

[7] Artoni P., Peccenini E., Pellicori V., Petrucci F., 2013. *La tavolozza di Au Velodrome.* To be published in Progetto Restauro, Ed. Il Prato, Padova.

[8] Bacci M., Picollo M., Trumpy G., Tsukada M., Kunzelman D., 2007. *Noninvasive identification of White Pigments on 20th-century oil paintings by using Fiber optics reflectance spectroscopy: Their Identification by means of Noninvasive Ultraviolet, Visibile, and Infrared Fiber Optic Reflectance Spectroscopy.* In: Journal of the American Institute for Conservation, **46**-1, pp. 27 - 37.

[9] Barnes N. F., 1939. *A spectrometric study of artist's pigment.* In: Technical studies in the field of the fine arts, **7**, pp. 120 - 130.

[10] Basilissi G., Boselli L., Carlesi S., Ciofi L., Cucci C., Picollo M., 2012. *Spettroscopia UV-Vis-NIR per lo studio di pigmenti verdi moderni.* In: AIAr, Proceedings of VII Archaeometry National Meeting, Modena, Patron Ed., Bologna, pp. 906 - 921.

[11] Berns R. S., Taplin L. A., Imai F. H., Day E. A., Day D. C., 2005. *A comparison of small-aperture and image-based spectrophotometry of paintings.* Studies in Conservation, **50**(4), pp. 253 - 266.

[12] Buccellati G., Marchi A., Ed., 2001. *Oltre il visibile - indagini riflettografiche.* University of Milano.

[13] Buxbaum G., 2008. *Industrial inorganic pigments.* Second edition. John Wiley & Sons.

[14] Cennini C., 1859. *Il libro dell'arte: o, Trattato della pittura.* Firenze, Felice Le Monnier.

[15] Daffara C., Pampaloni E., Pezzati L., Barucci M., Fontana R., 2010. *Scanning Multispectral IR Reflectography SMIRR: An advanced tool for art diagnostics.* In: Acc. Chem. Res., **43**(6), pp. 847 – 856.

[16] Delaney J.K., Walmsley E., Barrie B.H., Fletcher C.F., 2005. *Multispectral Imaging of Paintings in the Infrared to Detect and Map Blue Pigments.* In: NAS Sackler Scientific Examination of Art: Modern Techniques In Conservation and Analysis, The National Academies Press, Washington DC, pp. 120-135.

[17] Fischer C., Kakoulli I., 2006. *Multispectral and hyperspectral imaging technologies in conservation: current research and potential applications.* Studies in Conservation, **51**, pp. 3 - 16.

[18] Forina, M., Lanteri, S., Armanino, C., Casolino, C., Casale, M., Olivieri, P., 2011. *Chemometrics with PARVUS.* In: School of Chemometrics 2011, Genoa University, Italy, June 6^{th}- 9^{th} 2011.

[19] Goetz A.F.H., Vane G., Solomon J.E., Rock B.N., 1985. *Imaging Spectrometry for Earth Remote Sensing.* Sciences, **228**(4704), pp. 1147 - 1153.

[20] Konica Minolta, *Precise color communication. Color control from perception to instrumentation.* Konica Minolta, Japan. Available on site: http://www.konicaminolta.com/instruments/knowledge/color/index.html.

[21] Maltese C. Ed., 2005. *Le tecniche artistiche.* Mursia Ed., Milano, Italy.

[22] Matteini M., Moles A., 2004. *La Chimica nel restauro - I materiali dell'arte pittorica.* Nardini Ed., Firenze, Italy.

[23] Murtagh F., Heck A., 1987. *Multivariate Data Analysis.* Kluwer, Dordrecht.

[24] Oleari C., Ed., 1998. *Misurare il colore. - Spettrofotometria, fotometria e colorimetria. Fisiologia e percezione.* Hoepli Ed., Milano, Italy.

[25] Oleari C., Ed., 2008. *Misurare il colore. - Fisiologia della visione a colori. Fotometria - Colorimetria e norme internazionali. Second edition.* Hoepli Ed., Milano, Italy.

[26] Picollo M., Basilissi G., Cucci C., Stefani L., Tsukada M., *Ultraviolet, Visible and Near Infrared Reflectance Spectra of Modern Pictorial Materials in the 200-2500 nm range.* Institute of Applied Physics "Nello Carrara" (IFAC) of the National Research Council (CNR) of Italy, Firenze. Available on site: http://drs.ifac.cnr.it/info.php

[27] Picollo M., Bacci M., Magrini D., Radicati B., Trumpy G., Tsukada M., Kunzelman D., 2007. *Modern White Pigments: Their Identification by means of Noninvasive Ultraviolet, Visibile, and Infrared Fiber Optic Reflectance Spectroscopy.* In: Modern Paints Uncovered, Getty Conservation Institute, Los Angeles, pp. 118 - 128.

[28] Petrucci F., 2000. *Telerilevamento di spettri di riflettanza per la diagnostica di opere d'arte contemporanea.* In: SIOF, Conference proceedings of 1999 (Florence) and 2000 (Venice), *Colorimetry and cultural heritage*, Centro editoriale toscano, pp. 82 - 93.

[29] Petrucci F., Schwartzbaum P., Artoni P., Bussolari D., Caforio L., Fedi M.E., Mandò P.A., Peccenini E., Pellicori V., 2012. *At the cycle-Race Track: A non-invasive investigation of materials and pictorial technique.* In: Weddingen E. Ed., *Cycling, Cubo-Futurism and the Fourth Dimension. Jean Metzinger's At the Cycle-Race Track*, Catalogue of the exhibit, Peggy Guggenheim Collection, Venice, pp. 74 - 83.

[30] Principal Component Analysis (handhout). In: Junker B., Shalizi C.. Statistics 36-490: Undergraduate Research. Spring 2010, Carnegie Mellon Department of Statistics, Pittsburgh, PA.

[31] Rossi G., Iacomussi P., Sarotto M., Soardo P., 1998. *Misurazioni goniorifiettometriche per la colorimetria.* In: SIOF, Conference proceedings of the 1995, 1996 and 1998, *Proceedings of colorimetry 1998*, SIOF, pp. 71 - 86.

[32] Seccaroni C., Moioli P., 2002. *Fluorescenza X - Prontuario per l'analisi XRF portatile applicata a superfici policrome.* Nardini Ed., Firenze, Italy.

[33] Serway R.A., Jewett J.W., 2003. *Principi di fisica.* Second edition. EdiSES, Naples, Italy.

[34] Thoury M., Delaney J. K., de la Rie E. R., Palmer M., Morales K., Krueger J., 2011. *Near-infrared luminescence of cadmium pigments: In situ identification and mapping in paintings.* In: Applied Spectroscopy, **65**(8), pp. 939 - 951.

[35] van Alphen M., 1998. *Paint film Components.* National Health Monographs. General series N. 2.

[36] Vasari G., 1986 *Le vite de' più eccellenti pittori, scultori et architettori [Firenze 1550].* Bellosi L., Rossi A. Ed., Einaudi Ed., Torino, Italy.

[37] Verri G., Clementi C., Comelli D.; Cather S., Piqué F., 2008. *Correction of Ultraviolet-Induced Fluorescence Spectra for the Examination of Polychromy* Applied Spectroscopy, **62**(12), pp. 1295 - 1302.

[38] Verri G., 2009. *The spatial characterisation of Egyptian blue, Han blue and Han purple by photo-induced luminescence digital imaging.* In: Analytical and Bioanalytical Chemistry, **394**(4), pp. 1011 – 1021 [DOI 10.1007/s00216-009-2693-0].

[39] Volpin S., Appolonia L., 2002. *Le analisi di laboratorio applicate ai beni artisitici policromi.* Il Prato Ed., Padova, Italy.

[40] Wise, B.M., 2010. *Chemometrics I: Principal Components and Exploratory Data Analysis.* Eigenvector Research, Inc.. In: School of Multivariate Analysis for Novices, La Sapienza University of Rome, Taormina, Italy, September 23^{rd} – 25^{th} 2010.

Acknowledgements

I owe my deepest gratitude to my advisor Ferruccio Petrucci from the University of Ferrara, for the special advices, the availability, the endless patience and for giving me the opportunity to grow professionally.

It is a pleasure to thank Mauro Gambaccini, for offering me the opportunity of working at the Department of Physics and Earth Sciences of Ferrara University.

I would like to thank the services of Mechanical Design and Workshop, Electronics and Computing in the person of Stefano Chiozzi, Federico Evangelisti, Stefano Squerzanti of INFN Section of Ferrara, and Luca Landi of Ferrara University for their collaboration and valuable contribution to design and built of the Image Spectroscopy device.

I would also like to thank Irene Bortolotti for the realization of the Tele32 software, essential for the processing of the images captured by Image Spectroscopy.

A special thanks to Paul Schwartzbaum of the Solomon R. Guggenheim Foundation, New York, for his willingness and for giving us opportunities to study some of the paintings of the Peggy Guggenheim Collection of Venice.

I am also grateful to Paola Artoni of LANIAC, Non-invasive Analysis Laboratory for Ancient, modern and Contemporary works of Art of University of Verona, for providing the XRF instrumentation to analyze the Jean Metzinger's work.

A very special thanks goes out to the other members of my research group: Fauzia Albertin, Lara Boselli, Eva Peccenini and Flavia Tisato, for the useful scientific discussions, for their support and friendship.